Spatial Normalization and Averaging of Diffusion Tensor MRI Data Sets

Derek K. Jones,*,† Lewis D. Griffin,‡ Daniel C. Alexander,§ Marco Catani,*,¶
Mark A. Horsfield,† Robert Howard,* and Steve C. R. Williams‖

*Section of Old Age Psychiatry and ‖Neuroimaging Research Group, Institute of Psychiatry, De Crespigny Park, London SE5 8AF,
United Kingdom; †Division of Medical Physics, Leicester Royal Infirmary, Infirmary Square, Leicester LE1 5WW, United Kingdom;
‡Radiological Sciences, 5th Floor Thomas Guy House, Guy's Campus, London SE1 9RT, United Kingdom; §Department of
Computer Science, University College London, Gower Street, London WC1E 6BT, United Kingdom; and
¶Institute of Gerontology and Geriatrics, University of Perugia, Perugia, Italy

Diffusion tensor magnetic resonance imaging (DT-MRI) is unique in providing information about both the structural integrity and the orientation of white matter fibers *in vivo* and, through "tractography", revealing the trajectories of white matter tracts. DT-MRI is therefore a promising technique for detecting differences in white matter architecture between different subject populations. However, while studies involving analyses of group averages of scalar quantities derived from DT-MRI data have been performed, as yet there have been no similar studies involving the whole tensor. Here we present the first step towards realizing such a study, i.e., the spatial normalization of whole tensor data sets. The approach is illustrated by spatial normalization of 10 DT-MRI data sets to a standard anatomical template. Both qualitative and quantitative approaches are described for assessing the results of spatial normalization. Techniques are then described for combining the spatially normalized data sets according to three definitions of average, i.e., the mean, median, and mode of a distribution of tensors. The current absence of, and hence need for, appropriate statistical tests for comparison of results derived from group-averaged DT-MRI data sets is then discussed. Finally, the feasibility of performing tractography on the group-averaged DT-MRI data set is investigated and the possibility and implications of generating a generic map of brain connectivity from a group of subjects is considered. © 2002 Elsevier Science (USA)

Key Words: diffusion tensor; MRI; spatial normalization; coregistration; mean; median; mode; central tendency; fractional anisotropy; tractography; group mapping.

INTRODUCTION

Diffusion tensor magnetic resonance imaging (DT-MRI), developed by Basser *et al.* (1994), allows the diffusion tensor to be estimated noninvasively in each voxel of an MR data set, by acquiring a series of MR images sensitized to diffusion in different directions and fitting a tensor model to the data.

In the CSF-filled ventricles and in gray matter at the typical spatial resolution of DT-MRI data (2.5 × 2.5 × 2.5 mm), the diffusivity of water molecules is independent of the direction in which it is measured, i.e., it is isotropic. In the white matter, however, diffusion is much more hindered across a bundle of coherently ordered axons than when diffusing parallel to the long axes of the axons (Moseley *et al.,* 1990). Hence in white matter, diffusion cannot be characterized by a single scalar quantity and is better described by the tensor matrix formalism (Crank, 1962).

The degree to which the apparent diffusivity depends on the direction in which it is observed is characterized by the anisotropy of the diffusion tensor. Several quantitative measures of diffusion anisotropy have been proposed (e.g., Basser *et al.,* 1994; Basser and Pierpaoli, 1996; Pierpaoli and Basser, 1996), but the most robust are those that are independent of the orientation of the sample with respect to the measurement system and do not require rank sorting of the eigenvalues (Pierpaoli and Basser, 1996.).

Since the self-diffusivity of a water molecule is sensitive to changes in its local environment, the diffusion tensor acts as a probe of tissue architecture. This makes DT-MRI an attractive option for studying differences in white matter between different subject groups. Indeed, early reports looking at anisotropy measures *in vivo* suggest that DT-MRI can reveal differences between, for example, normal healthy volunteers and patients with amyotrophic lateral sclerosis (Ellis *et al.,* 1999; Glauche *et al.,* 2001), alcoholics (Hedehus *et al.,* 1999), dyslexics (Klingberg *et al.,* 2000), epileptics (Eriksson *et al.,* 1999, 2001; Rugg-Gunn *et al.,* 2001), and schizophrenics (Buchsbaum *et al.,* 1998;

Lim *et al.,* 1999; Pfefferbaum *et al.,* 1999; Foong *et al.,* 2000; Steel *et al.,* 2001; Agartz *et al.,* 2001) and may also reveal gender and age differences in normal healthy volunteers (Virta *et al.,* 1999).

Two approaches have generally been adopted for investigating intergroup anisotropy differences. The first involves manual placement of regions of interest (ROI) in the brain and recording the mean anisotropy within the ROI for each individual subject (e.g., Ellis *et al.,* 1999; Virta *et al.,* 1999; Foong *et al.,* 2000; Steel *et al.,* 2001). The second involves generation of a group-averaged data set and subsequent comparison of data either from within an ROI (e.g., Hedehus *et al.,* 1999; Klingberg *et al.,* 1999) or on a voxel-by-voxel statistical basis (e.g., Buchsbaum *et al.,* 1998; Eriksson *et al.,* 1999, 2001; Rugg-Gunn *et al.,* 2001; Glauche *et al.,* 2001). This latter approach relies on coregistration of data sets and a straightforward averaging of the scalar intensities within each voxel to create a group-averaged scalar data set.

In this study, we extend the concept of group averaging of *scalar* data to group averaging of *tensor* data and show how a group-averaged tensor data set can be created in a standard anatomical reference space. Methods are presented for generating not only the mean tensor within each voxel, but also the median and mode of the distribution of tensors within each voxel. We then assess how well results obtained in the average data set conform to results obtained in the individual brains and consider implications for group averaging of both scalar and tensor data in clinical studies. We also discuss how our findings impact of the validity of employing a single scalar quantity, such as anisotropy, for making inferences about connectivity in the human brain.

The use of DT-MRI data to reconstruct approximations to the pathways of white matter within the brain (i.e., "tractography") is a rapidly developing area of research in the field of DT-MRI (Basser, 1998; Jones *et al.,* 1998; Mori *et al.,* 1998, 1999; Poupon *et al.,* 1999, 2000; Jones *et al.,* 1999b; Conturo *et al.,* 1999; Basser *et al.,* 2000; Tuch *et al.,* 2000, 2001; Koch *et al.,* 2001; Parker *et al.,* 2001). There is clearly great potential for such a technique in studying differences in the topology of white matter tracts between populations. However, while studies involving group averaging of (scalar) anisotropy measures have been performed, tractography has been reported only on an individual subject basis. In this work, we investigate the possibility of performing tractography on a population-averaged diffusion tensor data set. Finally, we investigate the possibility of generating a "summary" tractography result for a group of subjects, i.e., a map that summarizes the trajectories of the major white matter pathways, as seen by DT-MRI, within a group of subjects. We refer to this group-averaged map as a "generic connectogram." The implications of using a generic connectogram in clinical studies are discussed.

METHOD

Data Acquisition

Eleven healthy male volunteers (age range 25 to 39 years; mean 33.3 ± 4.7 years) who were free of neurological and psychological symptoms, and who were not taking medication, were recruited to this study. Although 11 subjects were recruited, the averaging was performed on data from only 10 of these subjects (referred to here as the "source subjects"). Data from the 11th subject were used to create a template DT-MRI data set.

Diffusion-weighted magnetic resonance imaging data were acquired from each subject on a 1.5-T GE Signa NV/i LX system (General Electric, Milwaukee, WI) with actively shielded magnetic field gradients (maximum amplitude 40 mT m^{-1}). A standard quadrature birdcage head coil was used for both RF transmission and MR signal reception.

Data were acquired using a multislice peripherally gated EPI sequence, optimized for precise measurement of the water self-diffusion tensor in the human brain (Jones *et al.,* 1999a, 2002), from 60 contiguous near-axial slice locations with isotropic ($2.5 \times 2.5 \times 2.5$ mm) resolution. The echo time was 107 ms while the effective repetition time was 15 R-R intervals. The duration of the diffusion-encoding gradients was 17.3 ms, giving a maximum diffusion weighting of 1300 s mm^{-2}. Diffusion gradients were applied in 64 isotropically distributed orientations (Jones *et al.,* 1999a, 2002). The total data acquisition time was approximately 14 min.

Analysis of Diffusion-Weighted Data

The diffusion-weighted images were initially corrected for the effects of eddy-current-induced distortion using in-house software. In brief, a reference image was first constructed by calculating the mean intensity in each voxel from all the non-diffusion-weighted images. Next, for each diffusion-weighted image the downhill simplex method (Press *et al.,* 1992) was used to select the optimal magnification, shear, and displacement of the diffusion-weighted images in order to give the best registration with the reference image. The "mutual information" (Collingon *et al.,* 1995; Viola *et al.,* 1996) was used to assess the registration between the "reference" image and the corrected image.

Following correction of image distortion, the diffusion tensor, together with the computed T_2-weighted intensity that would be obtained in the absence of any diffusion weighting, was calculated for each voxel using multivariate linear regression after logarithmic

transformation of the signal intensities (Basser *et al.,* 1994). The tensor in each voxel was subsequently diagonalized to determine the eigenvectors and eigenvalues, and the eigenvector associated with the largest eigenvalue (which we refer to here as the "principal eigenvector"), the trace, and the fractional anisotropy (Basser and Pierpaoli, 1996) of the tensor in each voxel were determined.

Generation of a Diffusion Tensor Template in Standard Space

In order to obtain a group-averaged DT-MRI data set in a standard anatomical reference space, it was first necessary to generate a template DT-MRI data set in a standard anatomical space by coregistering with a standard MR brain template. The standard MR template used for this purpose was the T_2-weighted EPI template included as part of the functional imaging analysis software package SPM99 (Wellcome Department of Cognitive Neurology, Institute of Neurology, London, UK). One subject was identified from the group of 11 subjects (referred to here as "the 11th subject"), whose age was close to the mean age of the remaining 10 subjects (age of 11th subject 33 years, mean age 33.3 years), and his data set was used to create the DT-MRI template.

The computed T_2-weighted volume data set obtained as part of the diffusion tensor fitting procedure was masked from the background signal using steps (i)–(iii) of the brain extraction procedure described below. The data were then imported into SPM99 and the "Spatial Normalisation" feature was used to coregister this T_2-weighted volume with the T_2-weighted volume template supplied in SPM, using an affine transformation with 12 degrees of freedom (Friston *et al.,* 1995a,b). The affine transformation matrix thus obtained was then applied to the fractional anisotropy volume data set of the 11th subject—to create a "target" fractional anisotropy data template in a standard reference space.

Brain Extraction

The software used for coregistration of tensor data sets (Alexander *et al.,* 1999, 2001, 2002) has previously been found to provide the most robust results when all extraneous signals are removed from the data set (i.e., only those voxels containing signal from the brain are retained as part of the image). While this extraction could be performed manually by tracing the contours of the brain by hand for each image slice, we developed an automated approach, such that the segmentation of the brain was objective. The procedure can be broken down into four steps.

(i) For each subject, the mean signal intensity in the background of the computed T_2-weighted image was automatically determined by selecting a rectangle of 400 pixels, whose long axis was parallel to the phase-encoding direction (so as to avoid inclusion of any potential Nyquist ghosting artifacts), and computing the mean pixel intensity.

(ii) The initial stage of brain extraction was performed using the software package BET—Brain Extraction Tool, part of the Functional Software Library package (Oxford Centre for Functional Magnetic Resonance Imaging of the Brain, Oxford University, Oxford, UK). Essentially, the software employs a mesh that is molded to the surface of the brain using a series of adaptive rules and constraints and the MR data set segmented into "brain" (within the mesh) and "nonbrain" (outside of the mesh). (Note. A technical report giving full details of this procedure is available for download from http://www.fmrib.ox.ac.uk/analysis/research/bet.)

(iii) Following preliminary extraction, a simple connectivity algorithm based on intensity thresholding was applied. This step was necessary since the fractional anisotropy volume data set masked by the output of step (ii) was often found to have a few very bright (high anisotropy) voxels around the external surface of the brain—most likely as a result of partial volume effects. The threshold that gave the best results was empirically found to be 3.5 times the mean background intensity determined in step (i).

(iv) Finally, the extracted T_2-weighted volume was used as a binary mask on the tensor volume data set.

Spatial Normalization of Tensor Data Sets

For each of the 10 source subjects, the masked tensor volume data set was coregistered (using an affine registration with 12 degrees of freedom) to the template using the approach described by Alexander *et al.* (1999, 2001, 2002). This approach employs the AIR registration package (Woods *et al.,* 1998a,b) for coregistration, and the computed transformations thus obtained are applied to the DT-MRI volumes using the preservation of principal directions algorithm (Alexander *et al.,* 2001a), which has been shown to reorient each tensor correctly under nonrigid transformations.

The images used for coregistration were the fractional anisotropy images computed from the six elements of the tensor (Basser and Pierpaoli, 1996). This measure is rotationally invariant (Pierpaoli and Basser, 1996), and we were therefore justified in coregistering each tensor data set to the template tensor data set by matching image intensities based on the fractional anisotropy.

Measures of Central Tendency

Following coregistration of the data sets, the mean ($\langle \mathbf{D} \rangle_2$), median ($\langle \mathbf{D} \rangle_1$), and mode ($\langle \mathbf{D} \rangle_0$) of the distribution of tensors within each voxel were computed. These

statistical concepts—mean, median, and mode—are relevant not only to the usual case of samples of scalar data but also to more complex geometrical data (Pennec and Ayache, 1998). The key step in this extension is the redefinition of mean, median, and mode in a more abstract form. This was achieved by Fréchet (1948), who defined a continuum of central locations μ_r, where $r \in \Re^+$. The central location, μ_r, is defined as that location in the domain of the samples that minimizes the sum of the distances, raised to the power r, to the samples. So, for example, μ_2 is the element that is closest to the samples in a distance-squared sense; μ_1 is the element that is closest to the samples in an absolute-distance sense, etc. Such definitions seem to bear no relation to the familiar definitions of mean, median, and mode, but it can readily be shown (Griffin, 1997) that for scalar variables the Fréchet-defined μ_2 is the mean, μ_1 is the median, and (with appropriate taking of limits) μ_0 represents the mode(s).

To apply the Fréchet definitions to tensor data, a metric was required. We used the metric

$$d(\mathbf{A}, \mathbf{B}) := \sqrt{(\mathbf{A} - \mathbf{B}) : (\mathbf{A} - \mathbf{B})}, \tag{1}$$

where $\mathbf{A}$ and $\mathbf{B}$ are the two different tensors and the symbol : indicates the generalized tensor dot product between two tensors (Morse and Feschbach, 1953).

In expanded form, Eq. (1) is written as

$$d(\mathbf{A}, \mathbf{B}) = \sqrt{\begin{array}{c} (A_{11} - B_{11})^2 + (A_{22} - B_{22})^2 + (A_{33} - B_{33})^2 \\ + 2(A_{12} - B_{12})^2 + 2(A_{13} - B_{13})^2 + 2(A_{23} - B_{23})^2 \end{array}}. \tag{2}$$

We note that this metric is invariant to choice of coordinate system. Using this metric it can be shown that the Fréchet mean of a sample of tensors coincides with the more obvious definition of the mean of a sample of tensors, i.e., $\mu_2(\{\mathbf{D}_1, \ldots, \mathbf{D}_n\}) = (1/n)\sum_{i=1}^n \mathbf{D}_i$, so the mean was determined in this more obvious and rapid way. To calculate the median of a sample of tensors we started with the mean tensor and then used gradient descent on the absolute distance function $d_1(\mathbf{X}) = \sum_{i=1}^n d(\mathbf{X}, \mathbf{D}_i)$. To calculate the mode, we started with the median and then repeatedly used gradient descent on the r-distance function $d_r(\mathbf{X}) = \sum_{i=1}^n |d(\mathbf{X}, \mathbf{D}_i)|^r$. For the first gradient descent, r was set to 0.9, for the second 0.8, and so on. At the completion of the gradient descent with $r = 0.1$, the sample closest to $\mu_{0.1}$ was selected as the mode tensor.

It can be shown that the derivative of the r-distance function is never zero outside the convex hull (the smallest convex region containing the set of the samples) and therefore the minima of the r-distance function are all contained within the convex hull of the

samples. For tensors, this property guarantees that each of the Fréchet-defined mean, median, and mode tensors of a sample of positive definite tensors will always be positive definite.

The Fréchet approach to central locations also naturally gives rise to methods for calculating dispersion measures, as generalized in Eq. (3), i.e.,

$$S_r = \frac{1}{n} \sum_{i=1}^n |d(\mu_r, D_i)|^r. \tag{3}$$

Again, as the parameter r is varied, a family of dispersion measures is defined. Of most interest are S_2, which is the standard deviation, and S_1, which is the mean absolute deviation.

We note that we can determine the most typical tensor data set of a sample in the following manner. First, we define d_{ij} for a pair of images, i and j, as the sum over all voxels of the distance (measured using the metric in Eq. (1)), between the tensor from image i and the tensor from image j, i.e.,

$$d_{ij} = \sqrt{\sum_{\text{all voxels}} d(\mathbf{D}_i, \mathbf{D}_j)^2}. \tag{4}$$

For each data set, we then formulate the root-mean-square distance between the tensors in the voxels in the ith data set and equivalent voxels in the other data sets, i.e.,

$$c_i = \frac{\sqrt{\sum_{i=1, j\neq1}^n d_{ij}^2}}{n-1}. \tag{5}$$

The most representative data set of the sample is that data set with the lowest value of c_i.

Following computation of the three measures of central tendency, ($\langle \mathbf{D} \rangle_2$, $\langle \mathbf{D} \rangle_1$), and $\langle \mathbf{D} \rangle_0$, and determination of the most typical data set, $\mathbf{D}_{\text{typ}}$, tensors were diagonalized and their eigenvectors and eigenvalues computed, and images of fractional anisotropy (Basser and Pierpaoli, 1996) were created. Furthermore, color images showing the orientation of the principal eigenvector (the eigenvector associated with the largest eigenvalues) were created using the "absolute direction" scheme reported by Pajevic and Pierpaoli (1999a, 2000).

Assessment of Spatial Normalization

Several strategies were developed to assess the quality of spatial normalization:

Visual Inspection of Alignment of Principal Eigenvectors

For each subject, the in-plane orientation of the principal eigenvector in each voxel was visualized using a modified version of the "quiver" library function in the mathematical software package MATLAB (The Mathworks, Natick, MA). The orientation of a principal eigenvector was represented only for those tensors for which the fractional anisotropy was above a threshold, arbitarily chosen to be 0.15. The 10 fiber-orientation images were then superimposed to allow visual inspection of the alignment of the principal eigenvector within each voxel. We refer to this composite image as a "bow-tie" plot, on account of the appearance of the bar plots within each voxel when the orientational coherence of the principal eigenvectors is relatively high.

Quantitative Measures of Alignment of Principal Eigenvectors

The bow-tie plots were created to allow visual inspection of the alignment of principal eigenvectors of the individual tensors within each voxel and were not designed to provide anything more than a qualitative measure of the degree of alignment. In regions where orientational coherence is low, the images could prove to be cluttered and difficult to summarize. Furthermore, the plots allow visualization of the projection of the three-dimensional orientational information only onto a two-dimensional plane. We therefore sought to gain quantitative measures of the three-dimensional alignment of the principal eigenvectors in each voxel, by computing maps based on dyadic tensors formed from the principal eigenvectors. The underpinnings of this work are to be found in Bingham (1974) and later in Basser and Pajevic (2000).

Following the approach of Basser and Pajevic (2000), we calculated the mean dyadic tensor, $\langle \boldsymbol{\varepsilon}_j \boldsymbol{\varepsilon}_j^{\mathrm{T}} \rangle$, for the N subjects, in each voxel, where

$$\langle \boldsymbol{\varepsilon}_i \boldsymbol{\varepsilon}_i^{\mathrm{T}} \rangle = \left\langle \begin{pmatrix} \varepsilon_{ix}^2 & \varepsilon_{ix}\varepsilon_{iy} & \varepsilon_{ix}\varepsilon_{iz} \\ \varepsilon_{ix}\varepsilon_{iy} & \varepsilon_{iy}^2 & \varepsilon_{iy}\varepsilon_{iz} \\ \varepsilon_{ix}\varepsilon_{iz} & \varepsilon_{iy}\varepsilon_{iz} & \varepsilon_{iz}^2 \end{pmatrix} \right\rangle = \frac{1}{N} \sum_{j=1}^{N} \boldsymbol{\varepsilon}_i^j \boldsymbol{\varepsilon}_i^{j\mathrm{T}} \quad (6)$$

and ε_i^j is the ith component of the principal eigenvector in the voxel for the jth subject. We then computed the three eigenvalues of $\langle \varepsilon_i \varepsilon_i^{\mathrm{T}} \rangle$, assigned here as β_1, β_2, and β_3. (Note that for each individual tensor, there is only one non-zero eigenvalue. The eigenvector of the dyad which is associated with this eigenvalue is parallel to the eigenvector from which the dyad is formed.)

The measure we chose to assess the intersubject coherence of eigenvectors was formulated directly from the dyad dispersion measure proposed by Basser and Pajevic (2000), i.e.,

$$\sqrt{\frac{\beta_2 + \beta_3}{2\beta_1}}. \quad (7)$$

The intersubject coherence of eigenvectors in each voxel was derived by subtracting this measure from 1 to form the dyadic coherence, κ.

$$\kappa = \left(1 - \sqrt{\frac{\beta_2 + \beta_3}{2\beta_1}} \right). \quad (8)$$

When the different subjects' principal eigenvectors are randomly distributed, then $\beta_1 \approx \beta_2 \approx \beta_3$ and $\kappa \to 0$, and when the individual principal eigenvectors are perfectly aligned with the mean principal eigenvector, then $\beta_2 = \beta_3 = 0$ and $\kappa = 1$.

Scattergrams of Fractional Anisotropy and Dyadic Coherence, κ

To investigate the relationship between orientational coherence of principal eigenvectors and anisotropy, the image analysis package Analyze (Biomedical Imaging Resource, Mayo Foundation, Rochester, MN) was used to create scattergrams of fractional anisotropy of the mean tensor, $\langle \mathbf{D} \rangle_2$, and dyadic coherence, κ (formed according to Eq. (6)) for every image voxel.

Regions of the scattergram were manually selected to include voxels with (i) high fractional anisotropy and high dyadic coherence measure and (ii) low fractional anisotropy and high dyadic coherence measure. The boundaries for our definitions of "high" and "low" were arbitrary. The voxels within the different scattergram regions were then highlighted on the image of the fractional anisotropy of the mean tensor, using a different color for each "signature" to allow their topographical distribution to be visualized.

Variability of Tensors

Several measures were formulated to assess the variability of tensors by examining the scatter of tensors about the measures of central tendency. To assess the scatter of the tensors about the mean, $\langle \mathbf{D} \rangle_2$, the following measure, S_2, was constructed from Eq. (3),

$$S_2 = \sqrt{\frac{1}{N-1} \sum_{k=1}^{N} (\mathbf{D}_k - \langle \mathbf{D} \rangle_2) : (\mathbf{D}_k - \langle \mathbf{D} \rangle_2)}, \quad (9)$$

where N is the number of subjects and $(\mathbf{D}_k - \langle \mathbf{D} \rangle_2)$ is the tensor formed by subtracting the mean tensor, $\langle \mathbf{D} \rangle_2$, from the kth individual tensor, $\mathbf{D}_k$.

The expression in Eq. (9) will be recognized as being analogous to the unbiased estimate of the standard deviation of the tensors. However, since this measure depends on the magnitude of the tensors in a voxel, we

also calculated a normalized measure of scatter about the mean (analogous to a coefficient of variation), in which the normalization factor is the magnitude of the mean tensor, $\|\langle \mathbf{D} \rangle_2\| = \sqrt{\langle \mathbf{D} \rangle_2 : \langle \mathbf{D} \rangle_2}$, i.e.,

$$\bar{S}_2 = \frac{S_2}{\|\langle \mathbf{D} \rangle_2\|}. \qquad (10)$$

To assess dispersion about the median, the following measure is appropriate:

$$S_1 = \frac{1}{N-1} \sum_{k=1}^{N} \sqrt{(\mathbf{D}_k - \langle \mathbf{D} \rangle_1) : (\mathbf{D}_k - \langle \mathbf{D} \rangle_1)}. \qquad (11)$$

Again, a normalized form of S_1 is obtained by dividing by $\|\langle \mathbf{D} \rangle_1\|$ to give

$$\bar{S}_1 = \frac{S_1}{\|\langle \mathbf{D} \rangle_1\|}. \qquad (12)$$

Tractography

To investigate the feasibility of creating a generic connectogram and to determine how well a tractography result obtained from an averaged data set would represent results obtained from individual subjects, we performed tractography in both a typical subject and the averaged data set. The software for estimating the trajectories of tracts from diffusion tensor data was written in the C programming language and based on the procedure originally described by Basser (1998).

Generating a Continuous Description of the Tensor Field

The first step involved generating a continuous description of the diffusion tensor field from the voxelwise discrete estimates by B-spline fitting a series of basis functions to the elements of the tensor matrices (Aldroubi and Basser, 1999; Pajevic *et al.,* 2001). This procedure allows rapid evaluation of the diffusion tensor at any arbitrary location within the imaged volume and also permits smoothing of the tensor field (Aldroubi and Basser, 1999).

A set of locations for the initiation of the tracking algorithm (the "seed points") was first selected on the fractional anisotropy images (see below). For each of these seed points, the diffusion tensor was estimated and diagonalized to determine the principal eigenvector. The tracking algorithm then moved a distance of 0.5 mm (arbitrarily chosen) along this direction. The diffusion tensor was determined at this new location (obtained from the continuous description of the tensor field) and the orientation of its principal eigenvector

estimated. The algorithm then moved a further 0.5 mm along this new direction. A pathway was traced out in this manner until the fractional anisotropy of the tensor fell below a fixed arbitrary threshold (set to 0.15, unless mentioned otherwise). The procedure was then repeated by tracking in the direction opposite to the first step at the seed point, in order to reconstruct the whole tract passing through the seed point.

Seed-Point Selection

As mentioned above, the first step toward generating images of fasciculi was to define starting regions for the tracking procedure. For each fasciculus, a ROI was defined on the anisotropy image in a region where the fasciculus is well defined, according to previous neuroanatomy works (Dejerine, 1895; Crosby *et al.,* 1962). In order to pick out tracts of a specific fasciculus, which may run close to tracts belonging to other fasciculi, it was sometimes necessary to employ a "two region of interest" approach, in a manner similar to that reported by Conturo *et al.,* (1999). The procedure was to place a second ROI such that it also contained a section of the fasciculus of interest, but at a distance from the first region of interest. Only those tracts whose paths connected both regions of interest were retained, and in this way it was possible to select exclusively those fibers belonging to the desired fasciculus. The typical time for computation of the trajectories from a hundred seed points was 20 s, running on a Sun Sparcstation Ultra 140.

The fasciculi studied for this work were the corpus callosum, the uncinate fasciculi, and the inferior occipitofrontal fasciculi. Tractography was also performed in a region of frontal white matter where the intersubject intravoxel orientation coherence of principal eigenvectors was low. Regions of interest were defined on the fractional anisotropy image computed from the mean data set, $(\langle \mathbf{D} \rangle_2)$, and tractography was performed. The same regions of interest were then used for initialization of tractography in an individual subject, so that results obtained from an individual and a group-averaged data set could be compared directly. For some fasciculi, the anisotropy threshold was varied and tractography repeated in order to view the effects of different anisotropy thresholds within the average and individual data sets (see Results).

Display of Derived Tracts

At the completion of tracking, a list of points which lay at 0.5-mm intervals along the pathway traced out was generated. A three-dimensional representation of the pathways was then generated by creating a set of polygons with circular cross section, and fixed radius, to connect up the points, using MATLAB. The use of "stream tubes" to visualize white matter trajectories in this way was first reported by Zhang *et al.,* (2000). The
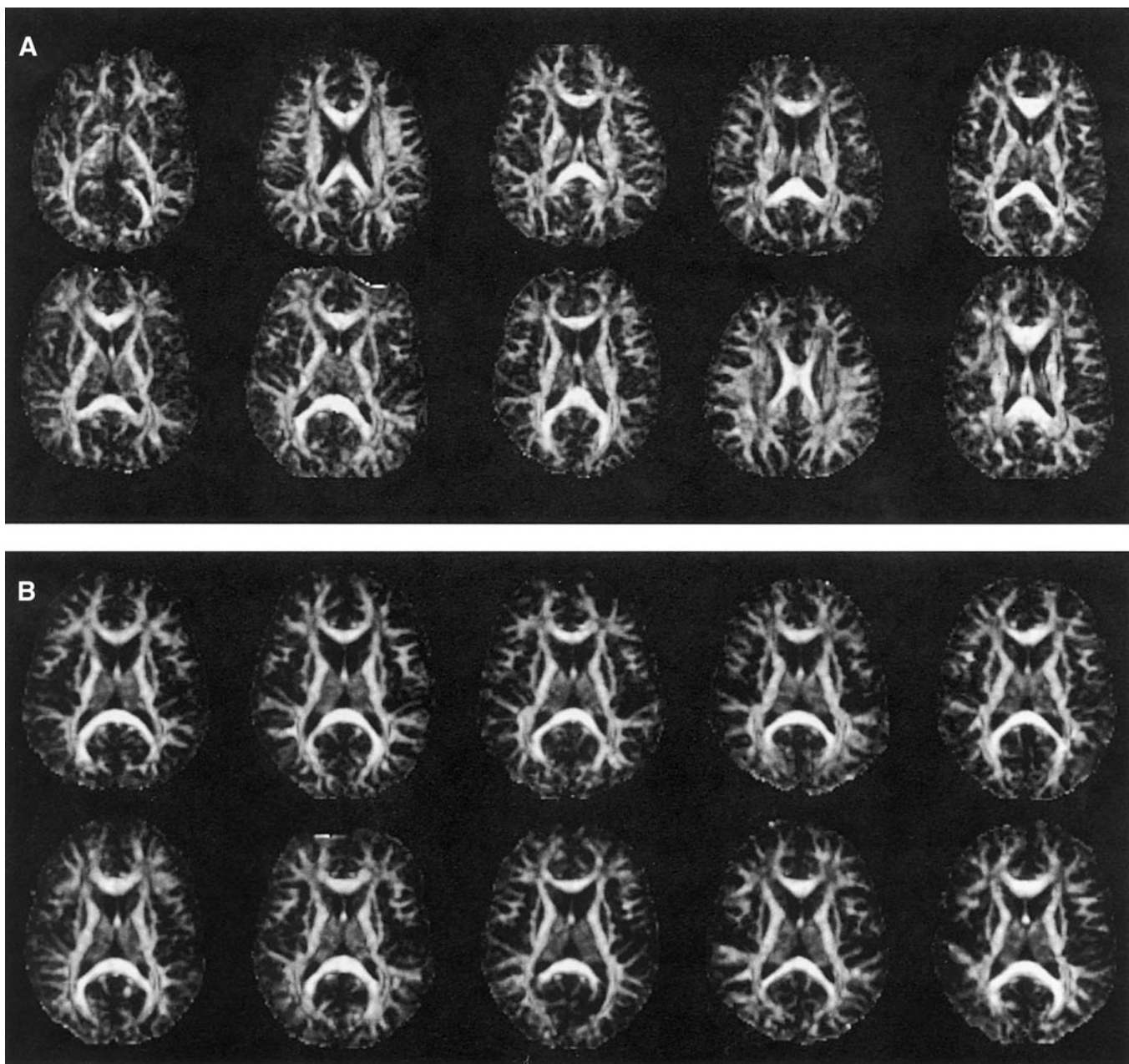
FIG. 1. Spatial normalization of diffusion tensor data sets. For illustrative purposes, the 36th slice from the 60-slice fractional anisotropy data set of each subject is shown both (A) before spatial normalization and (B) after spatial normalization.

rendered data could be rotated about any axis to permit viewing of the tracts from any angle.

RESULTS

Figure 1 shows one slice (slice 36) of the 60-slice fractional anisotropy data sets obtained from each of the 10 subjects both before and after spatial normalization and serves to illustrate that the registration was at least coarsely effective and did not fail across any of the subjects. Note that the variation in geometry and location of white matter structures appears to be greater in peripheral (subcortical) regions of the brain compared to the major and more centrally located structures.

Figure 2 illustrates the averaging procedure detailed under Measures of Central Tendency. The figure shows averaging of the 10 tensors for a voxel in which the normalized standard deviation of the tensors about the mean, $\bar{S}_2$, is 26%. This is typical of the scatter present across the 10 registered data sets: 40% of voxels have a normalized standard deviation greater than this. The
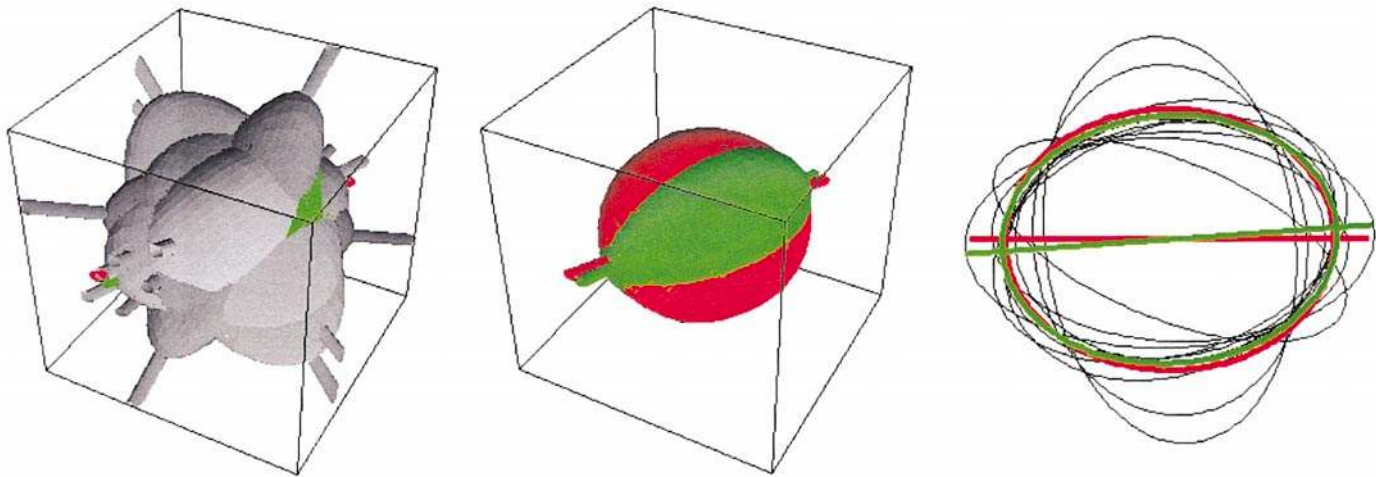
FIG. 2. Averaging of 10 tensors from a typical voxel in the data set. Each tensor is represented as an ellipsoid. The left shows the 10 individual tensors in gray, the mean tensor in red, and the median tensor in green. The principal eigenvector of each tensor is shown as a cylinder. The middle shows only the mean and median tensors. The right shows the cross section with the plane containing the principal eigenvectors of the mean and median tensor.

normalized difference between the mean and the median tensors, $(d(\langle D \rangle_2, \langle D \rangle_1))/\|(1/2)(\langle D \rangle_2 + \langle D \rangle_1)\| = 5\%$, is also typical: 40% of voxels have a greater fractional difference between the mean and the median tensors.

The fractional anisotropy of the mean tensor ($\langle \mathbf{D} \rangle_2$) data set is shown in Fig. 3a, while the orientation of the principal eigenvector is shown in Fig. 3b. Note that some relatively small structures are clearly delineated. For example, the motor fibers and sensory fibers are individually seen in the pons on the anisotropy image (Fig. 3a) and the transverse pontine fibers are readily seen on the fiber orientation image (Fig. 3b) in the last column of row 1 and first column of row 2. There is also some preservation of anisotropy information in subcortical regions (third row of Fig. 3a and 3b).

Figure 4 compares the fractional anisotropy images computed from an individual tensor data set and from the mean tensor data set. The effect of averaging in computation of the mean tensor data set clearly produces a smoother anisotropy image. As would be expected from inspection of Fig. 1B, in central major white matter structures (such as the corpus callosum and cingulum), the anisotropy data computed from the mean tensor data set appear to provide a fair representation of the anisotropy information contained in the individual tensor data set. However, as also expected from Fig. 1B, while anisotropy information in subcortical regions is preserved to a certain extent in the mean tensor data set, the fine detail of some of the smaller association and "U" fibers has been blurred.

Figure 5 allows comparison of results obtained from the mean, median, and mode tensor data sets, together with results obtained from the most typical subject, $\mathbf{D}_{typ}$. While there are no differences, at least discernible

by eye, between the results obtained from the mean and from the median tensor data sets the results obtained from the mode tensor data set appear "grainy," most likely as a direct consequence of computing a mode for the limited number of subjects used in this study.

Figure 6a shows an image of the normalized measure of scatter about the mean of the distribution, $\bar{S}_2$, for 16 slice locations (slice separation 7.5 mm). The images tend to be brighter at interfaces between different tissue types, for example at the interface of highly anisotropic white matter tissue with gray matter or at the interface of CSF-filled spaces with parenchyma, most likely reflecting imperfect coregistration of these boundaries across the subjects. In the white matter, the images tend to be brighter in more peripheral subcortical regions, most likely attributable to the greater intersubject anatomical variation in these areas. The centers of the fluid-filled lateral ventricles have the lowest intensity since these represent fairly homogeneous regions consisting of nearly isotropic tensors (any anisotropy being a result of noise). Slight misregistration in these regions would still lead to similar tensors being averaged.

Figure 6b shows a histogram of the scatter about the mean of the distribution for the whole brain, expressed as a percentage (i.e., $\bar{S}_2 \times 100$). The peak of this histogram is at about 22%, but there is a substantial number of voxels in which the coefficient of variation is larger.

Figures 7–10 allow visual inspection of the alignment of the principal eigenvectors in each voxel across the 10 subjects, using the bow-tie plots. A high degree of alignment is seen in the genu, body, and splenium of the corpus callosum (Figs. 7 and 8 respectively). How-
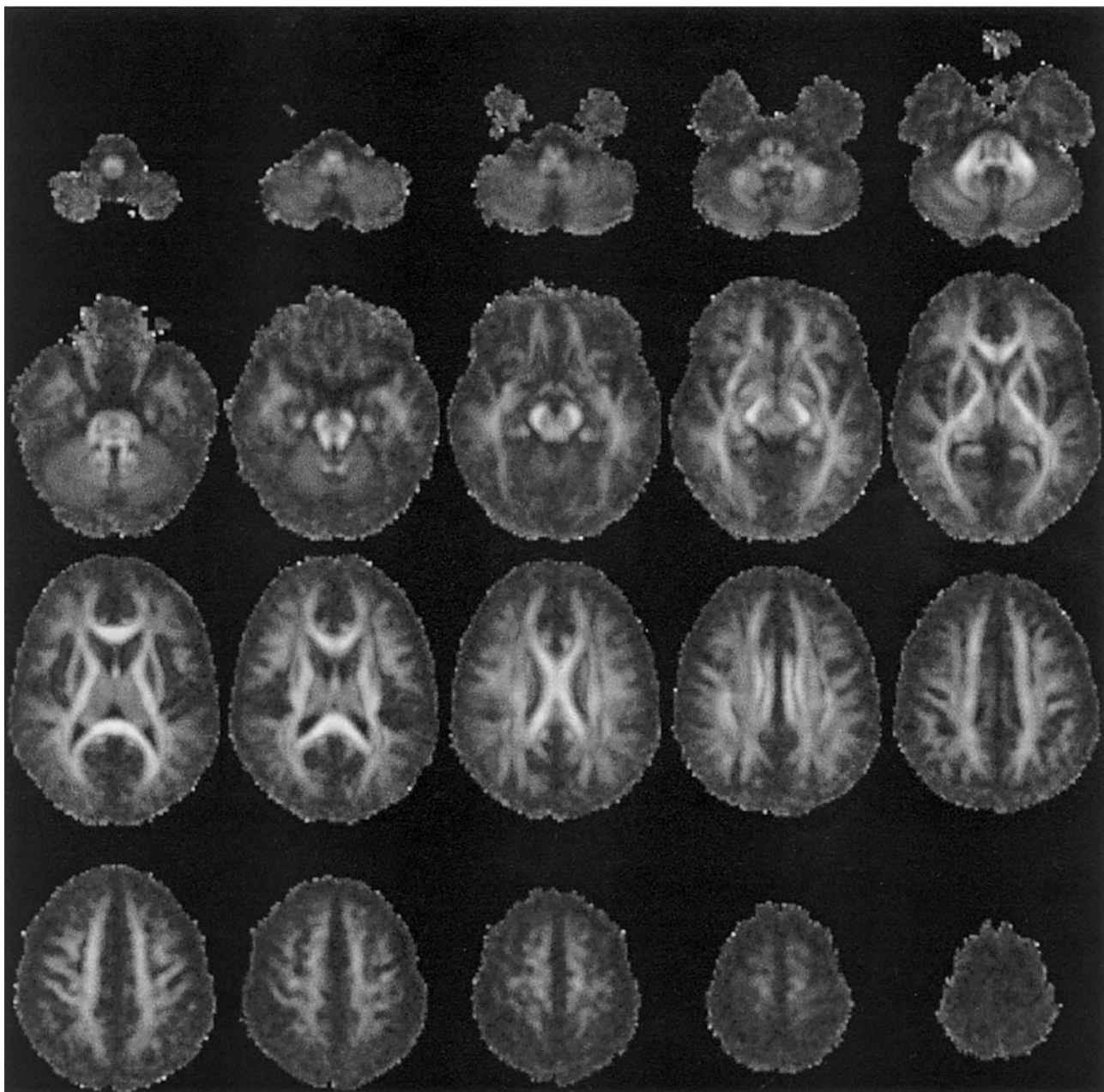
A

FIG. 3. (A) Fractional anisotropy images computed from the mean of the 10 spatially normalized diffusion tensor data sets. Every third slice is shown, starting at slice 3 of the 60-slice data set. Note the preservation of anisotropy information in relatively small structures such as the motor and sensory fibers in the pons and the cingulum bundle. (B) Fiber orientation images formed according to the "absolute" direction scheme. Fibers which are predominantly oriented left–right are shown in red, anterior–posterior fibers are shown in green, and superior–inferior images are shown in blue. The intensity in each voxel is modulated by the fractional anisotropy of the tensor

ever, Figs. 9A, 9B, and 9C show the orientations of the principal eigenvectors in frontal white matter, in a region similar to where previous studies have looked for intergroup differences in anisotropy measures (e.g., Steel *et al.,* 2001, compared anisotropy in regions of interest in this region to compare white matter integrity between schizophrenic patients and control sub-

jects). In comparison to the pattern seen in the corpus callosum (Figs. 7 and 8), the orientational coherence of the principal eigenvectors is very low, and the bow-tie plots in each voxel bear more resemblance to a star, reflecting a wide range of orientations of the principal eigenvectors in the voxel. This pattern is even more accentuated in Figs. 9D, 9E, and 9F, which show the
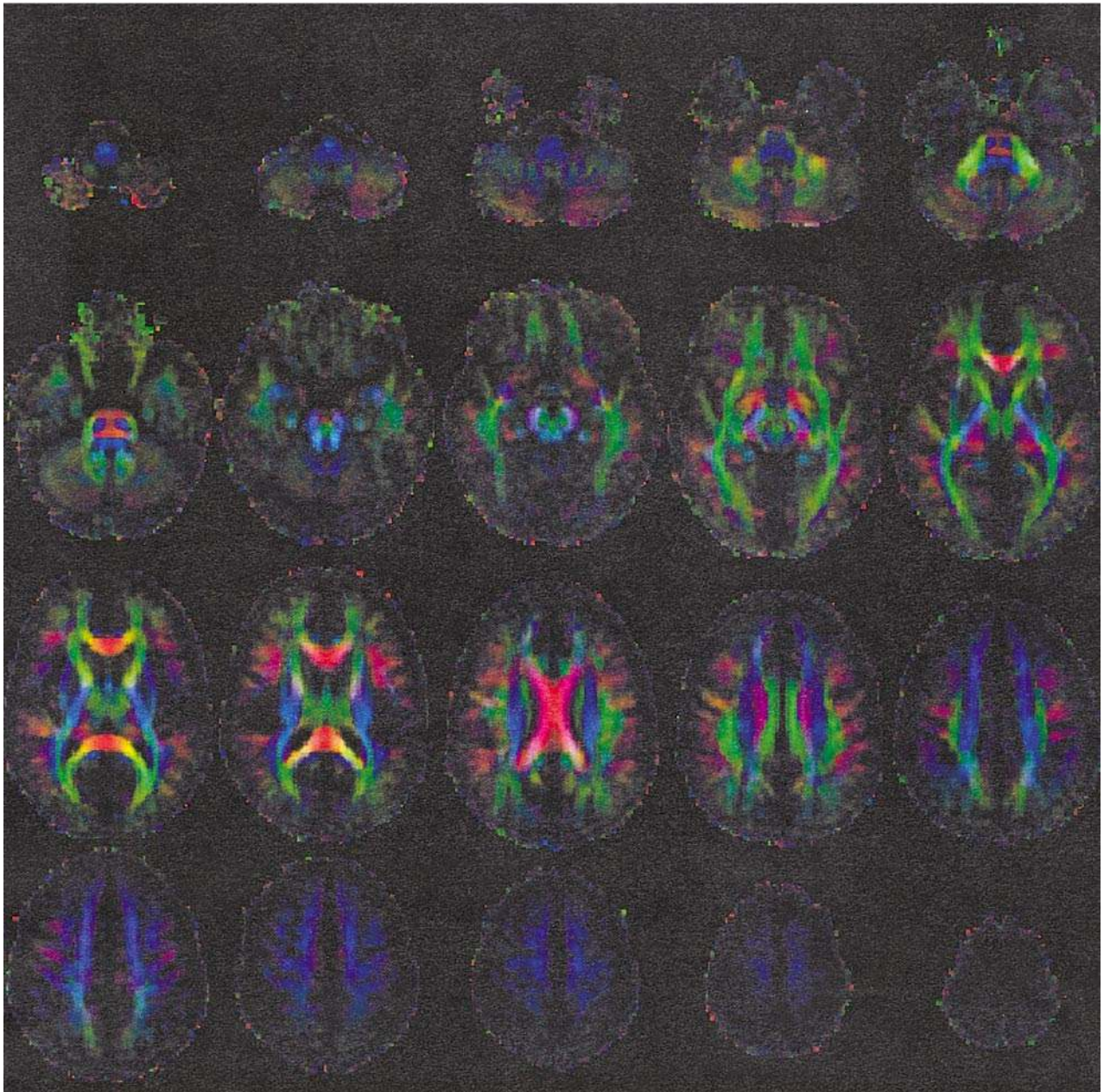
FIG. 3—*Continued*

principal eigenvectors in a region of subcortical white matter in the left hemisphere.

Figure 10 shows a band of high coherence of eigenvectors passing between the frontal and the temporal lobes. This is in the region of the uncinate and inferior fronto-occipital fasciculi, suggesting that attempts to track frontotemporal connections in the average brain may be successful and that the result would be representative of the results obtained from individual subjects.

Figure 11 shows every third slice of the 60-slice image of dyadic coherence, κ, formed according to Eq. (6). While the bow-tie plots in Figs. 7–10 allow the actual pattern of eigenvectors to be visualized, the dyadic coherence image provides a more readily interpretable "summary" of intravoxel alignment of the principal eigenvectors. The image is generally brighter in the central portion of the brain, suggesting better coregistration of the tensors in those voxels, possibly as a consequence of the spatial normalization transforma-
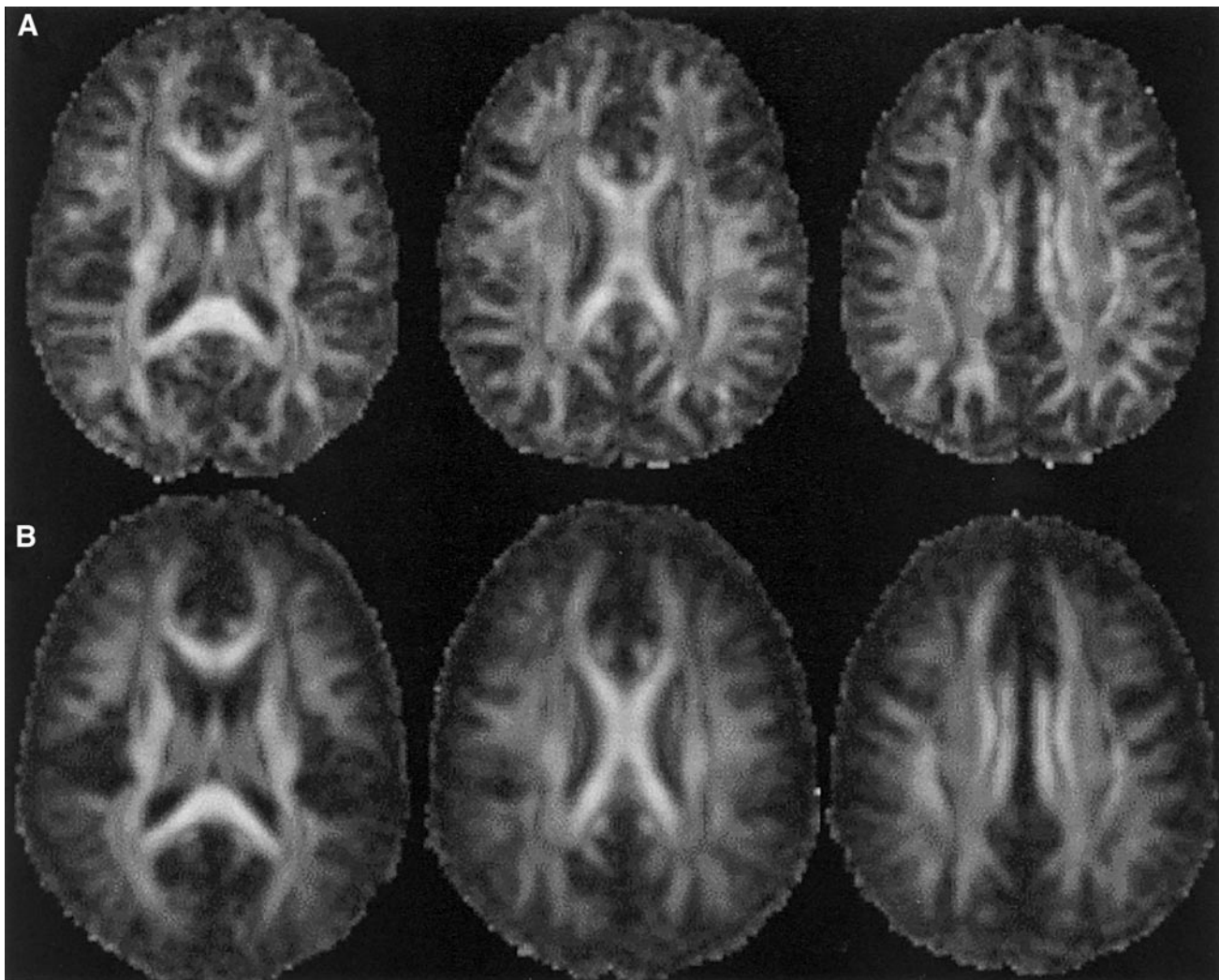
FIG. 4. Comparison of fractional anisotropy data obtained from (A) an individual tensor data set and (B) the group mean tensor data set. Three slice locations are shown, at the level of the splenium, body of corpus callosum, and cingulum.

tion employed in this work or there is generally greater coherence in these central structures across subjects.

Figure 12 shows the scattergram of the dyadic coherence and fractional anisotropy data. Two ROIs have been drawn on the scattergram to select all regions of "high" dyadic coherence. As expected (from Fig. 11), the voxels within these ROIs are almost all centrally located. The ROI shown in red was drawn to highlight those voxels with high dyadic coherence and high fractional anisotropy. These voxels are primarily located within the major centrally located white matter fasciculi (the genu, splenium, and internal capsule). The green ROI was drawn to select the section of the scattergram with high dyadic coherence, but "low" anisotropy (again, the boundaries of this ROI were arbitrarily chosen). This produced the intriguing result that the majority of the voxels that have high dyadic coherence and low anisotropy are located within certain parts of the thalamus. The bow-tie plot in Fig. 13

confirms this finding, i.e., a remarkable degree of alignment of the principal eigenvectors is seen within the thalamus. Note that in Fig. 12, there are regions within the thalamus where voxels have been highlighted and regions where they have not and there appears to be a high degree of symmetry about the midline.

Figure 14 shows tractography results obtained from the single and mean tensor data sets. The tracking result obtained by initiating tracking in the body of the corpus callosum (Fig. 14a) from the mean tensor data set is consistent with the result obtained from the individual subject. This is most likely attributable to the high anisotropy of this structure and its central location within the brain and was expected from the bow tie plot in Fig. 8. However, it is noticeable that in some regions, reconstructed tracts extend a little farther toward the cortex in the mean brain. Also, the routes of some of the computed tracts appear less tor-
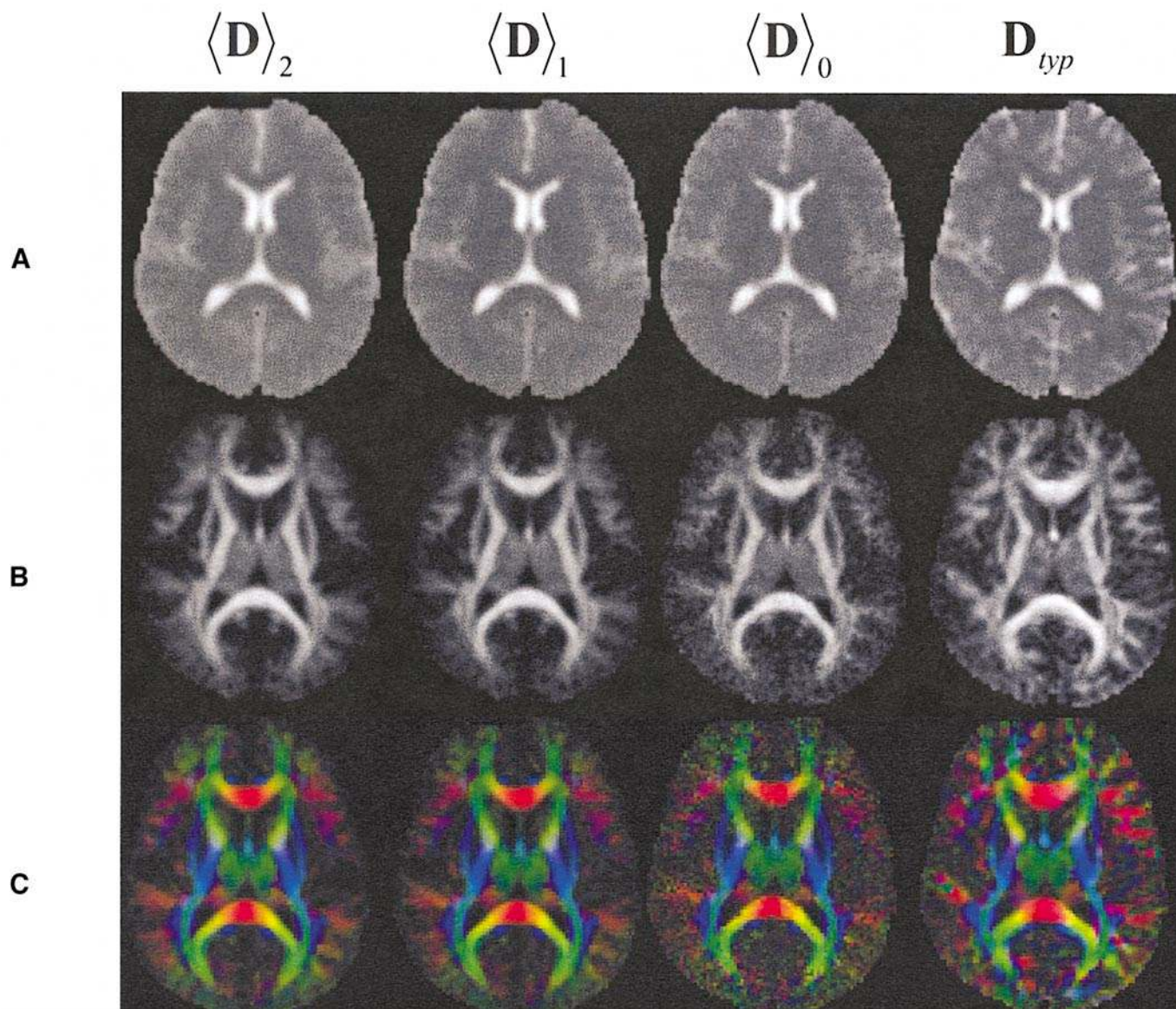
FIG. 5. Comparison of results obtained from the mean tensor, $\langle \mathbf{D} \rangle_2$, median tensor, $\langle \mathbf{D} \rangle_1$, and mode tensor, $\langle \mathbf{D} \rangle_0$, together with results from a typical individual subject, $\mathbf{D}_{typ}$. The mean diffusivity (A), fractional anisotropy (B), and orientational information (C) are shown for the same slice.

tuous in the mean brain than in the individual brain toward their termination points, most likely attributable to the averaging procedure.

Figure 14b shows the effect of varying the anisotropy threshold on tractography results obtained in the anterior forcep of the corpus callosum in both the individual brain and the mean brain. As expected from the bow-tie plots in Figs. 7D–7F, the tractography results obtained within the central portion of the anterior forcep in the individual and mean brain appear to be in good agreement. This suggests that, at least in this section of the structure, the results obtained in the mean brain can be used to summarize results obtained in the individual brains. However, also as expected

from the bow-tie plots, results obtained in the end termini differ strongly between the two data sets. While there appear to be fewer spurious reconstructions of tracts in the mean averaged brain than in the individual brain at an anisotropy threshold of 0.20, for example, the tracts terminate prematurely in the mean brain. When the anisotropy threshold is lowered, the number of spurious reconstructions of tracts appears to increase in the individual data set, while the fine detail of what appears to be end termini of the reconstructed tracts in the mean data set is increasingly revealed. Visual comparison of the end termini (or rather what we have deemed to represent end termini) in the mean and individual brains reveals marked differences in
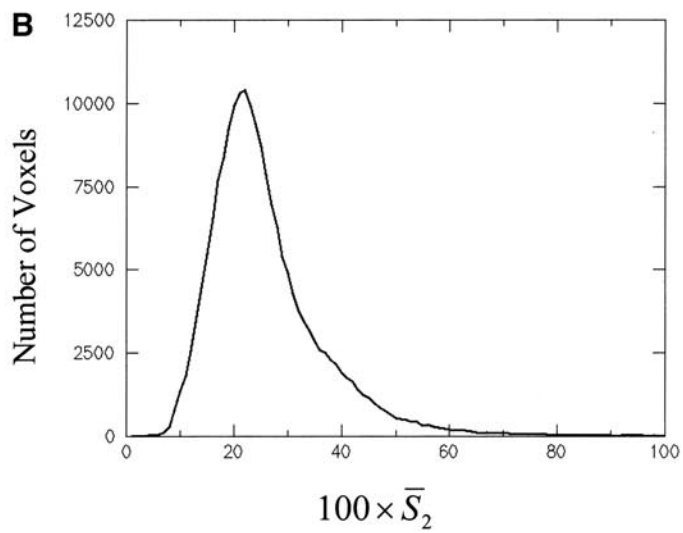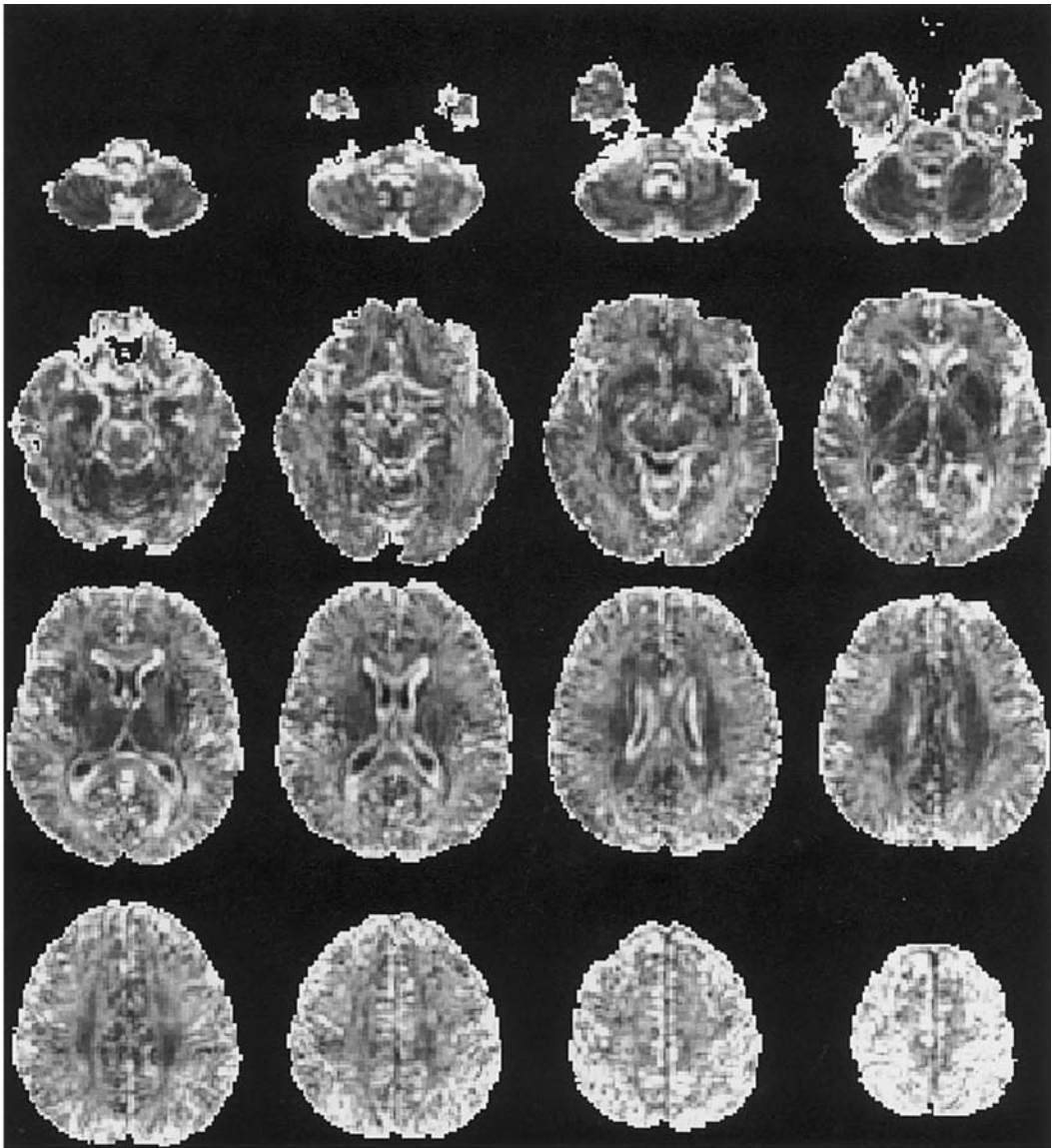
FIG. 6. (A) Map of normalized standard deviation, $\bar{S}_2$, at 16 slice locations (separation of slices 7.5 mm). (B) Histogram of $\bar{S}_2$, (expressed as a percentage) formed from the whole brain.
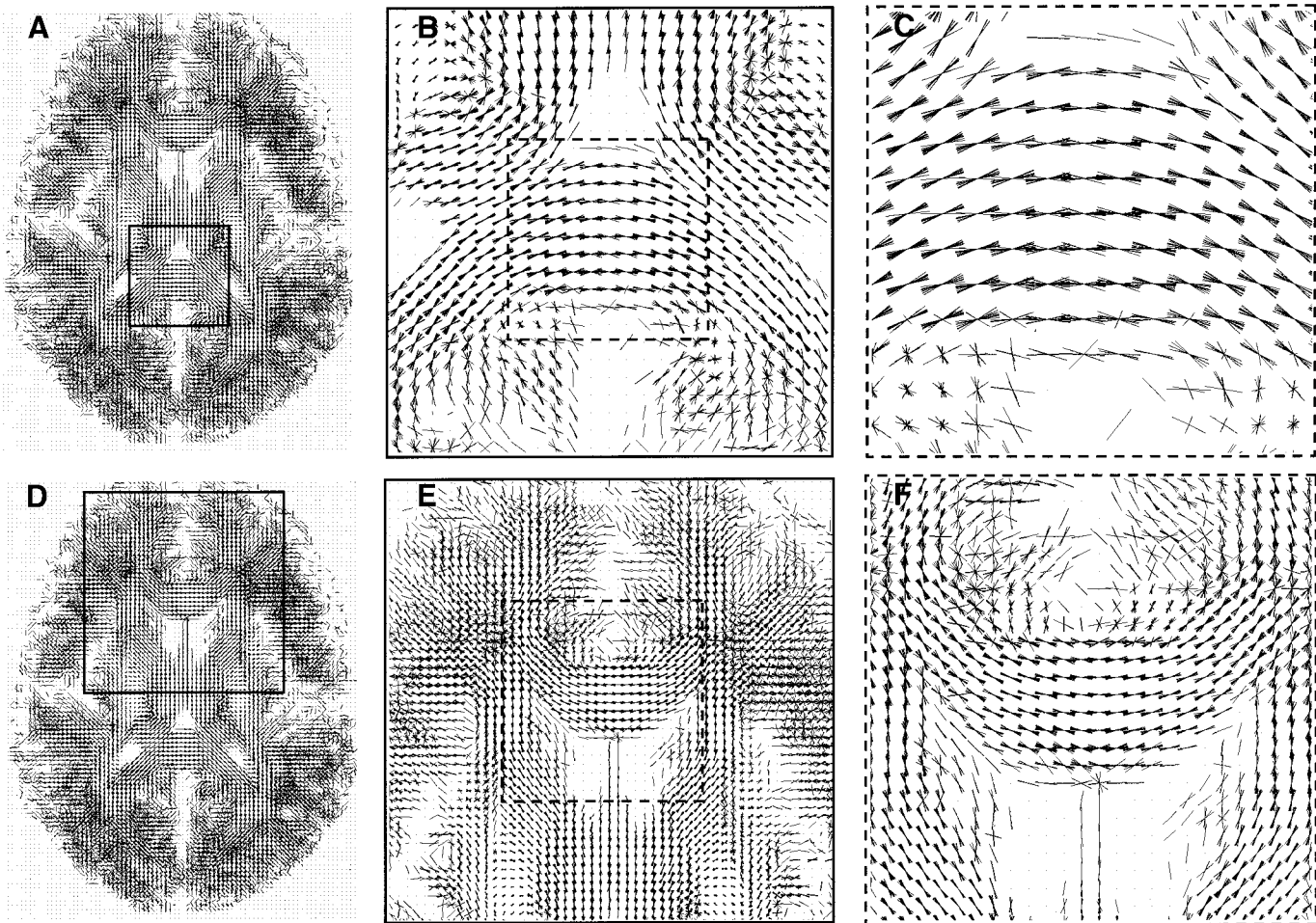
FIG. 7. Bow-tie plot showing orientational coherence of the principal eigenvectors in each voxel, across the 10 subjects, at different resolutions in the splenium (A–C) and genu (D–E) of the corpus callosum. The zoomed regions are indicated by the squares.

tract topology. This suggests that tractography results in such regions, obtained from the mean of a group of affine-registered data sets, provide a poor approximation of the results obtained in the individual data sets.

Figure 14c shows tractography results obtained from the uncinate and inferior occipitofrontal fasciculi. The results are consistent with known anatomy, i.e., coherently organized fasciculi running parallel to one another, with one fasciculus connecting the frontal and temporal lobes (the uncinate fasciculus) and the other fasciculus running between the frontal and the occipital lobes (the inferior occipitofrontal fasciculus). The results obtained in the average and individual brains are remarkably similar in their topologies, which was to be anticipated from the regions of high coherence of the bow-tie plot in Fig. 10.

Figure 14d shows results obtained in a region of frontal white matter where the intersubject intravoxel orientational coherence of principal eigenvectors is low. On a gross level, the results obtained in the individual and mean brain are similar. However, there is

an additional "high-frequency" component in the results in the individual brain that has not been preserved in the results obtained from the mean brain.

DISCUSSION

Mean, Median, and Mode Tensors

The mean of a distribution is one of the most familiar summary statistics for a distribution and the most often adopted by the neuroimaging community. However, in cases in which there may be statistical outliers, the benefits of examining the median of a distribution are well known. To the best of our knowledge, this is the first time that a method for computing the median (and indeed the mode) of a distribution of second-rank tensors has been formulated.

The mode of the distribution is likely to be a useful measure only in a very much larger cohort of subjects than the limited number presented in this study ($n =$ 10). This was reflected by the "grainy" appearance of
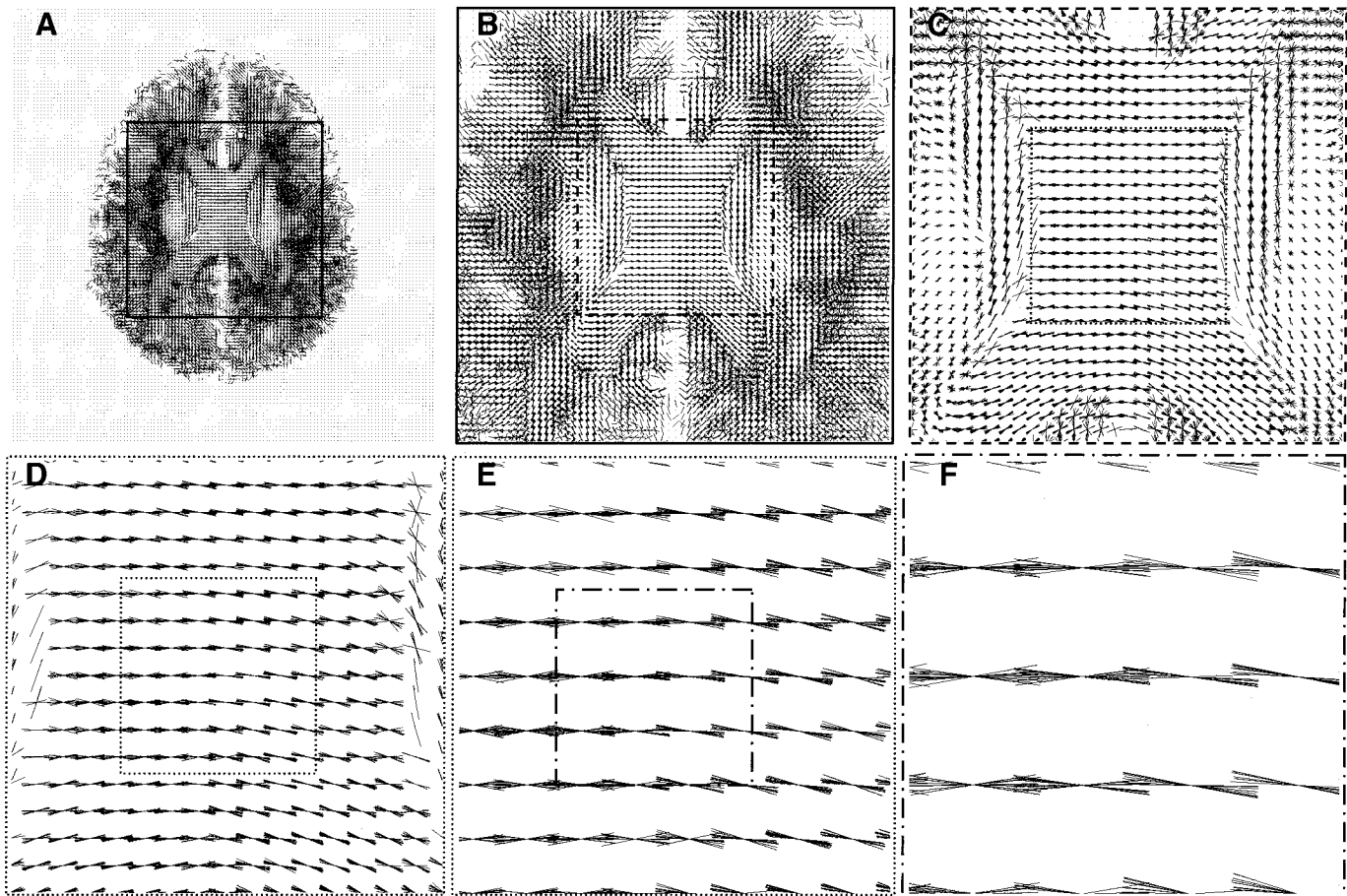
FIG. 8. Bow-tie plot in the body of the corpus callosum at different resolutions. The square in (A) shows the approximate location of the zoomed region shown in (B), selected to examine orientational coherence in the body of the corpus callosum. The region enclosed by the square in (B) has been enlarged in (C) and so on. Even at high resolution, the orientational coherence of the eigenvectors in the body of the corpus callosum appears high.

the mode of the tensor distribution obtained from this work. However, this approach was included in this work for the sake of completeness.

Tensor Dispersion Measures

Maps of the tensor dispersion measures, such as the maps of normalized standard deviation, $\bar{S}_2$, presented in Fig. 6, provide a useful tool for improving the robustness of region-of-interest analyses. The most representative voxels within a structure are those that possess the lowest intravoxel dispersion of tensors across the subjects. Therefore, by using the maps of tensor dispersion as an aid to placing the ROIs (i.e., in regions where the map of $\bar{S}_2$ is darkest, for example), one can be sure that the most representative voxels, and those that have been least contaminated by partial volume effects, have been selected.

Statistical Analysis of Group-Averaged Tensor Data Sets

In this work, we have demonstrated spatial normalization and averaging of DT-MRI data sets into a stan-

dard anatomical space and outlined a strategy for assessing the scatter of tensors and their principal eigenvectors.

One of our current aims is to develop robust methods for performing statistical comparisons of spatially normalized and group-averaged DT-MRI data sets. Scalar, vector, and tensor data are now available for group comparison. So far, only group analyses of scalar variables derived from the diffusion tensor have been reported. One approach has been to borrow the technique of statistical parametric mapping from functional MRI research (Friston *et al.,* 1995a,b) and apply it to group studies of diffusion anisotropy (Buchsbaum *et al.,* 1998; Eriksson *et al.,* 1999, 2001; Rugg-Gunn *et al.,* 2001; Glauche *et al.,* 2001). However, before conclusions about the robustness of such an approach can be made, the statistical distributions of the underlying data must be understood. While the statistical distribution of the elements of the diffusion tensor within a region of interest with spatially uniform diffusion properties has been characterized (Pajevic and Basser, 1999), no
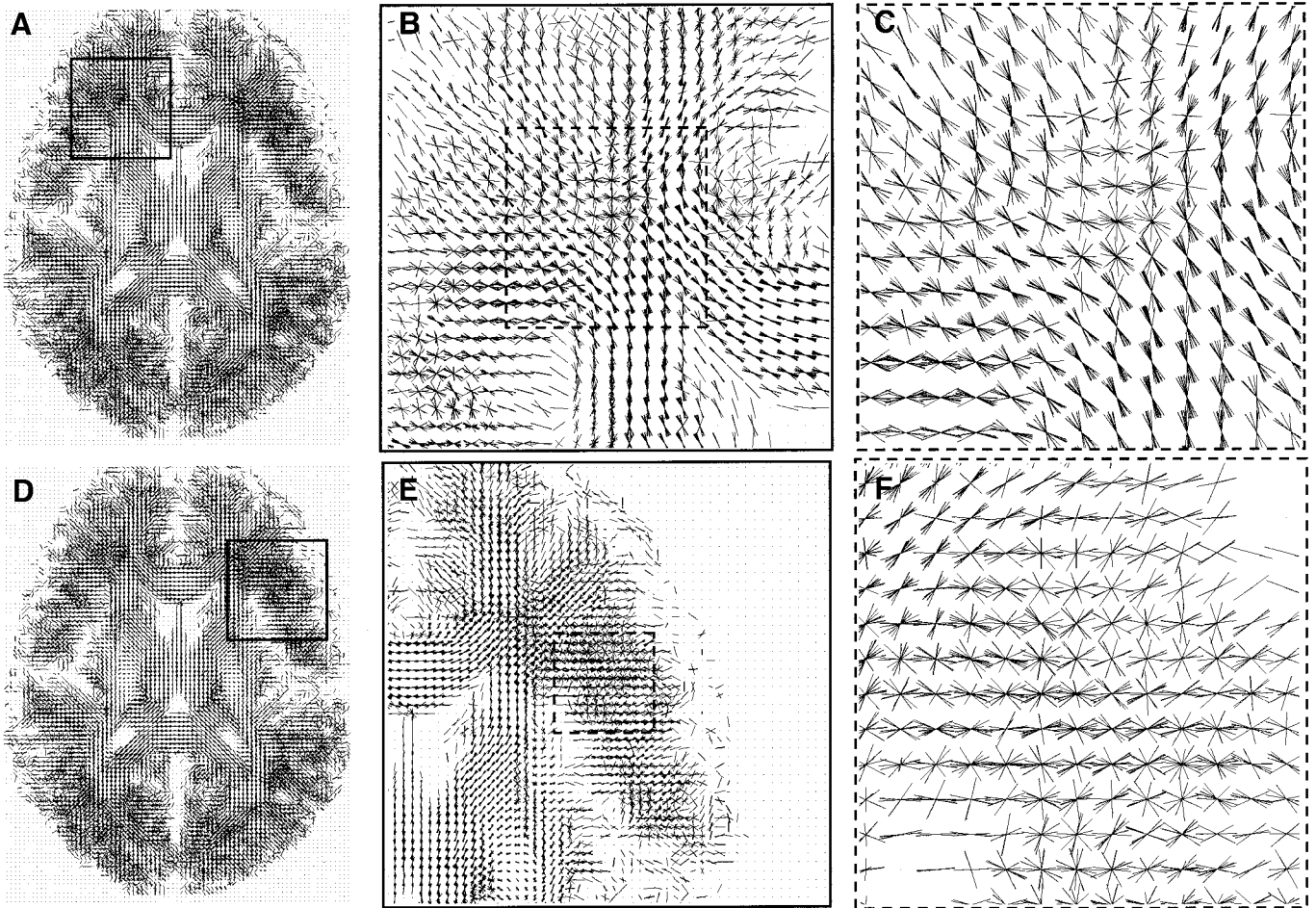
FIG. 9. Bow-tie plots of the principal eigenvectors in the frontal white matter (A–C) and subcortical white matter (D–F).

investigation into the statistical distribution of the moments of the diffusion tensor (second order and higher) has been reported in the DT-MRI literature. It may be that new statistical techniques need to be developed for group analyses of higher order moments of the diffusion tensor (reflecting the anisotropy, skewness, and kurtosis), perhaps employing nonparametric approaches (e.g., Holmes *et al.,* 1996).
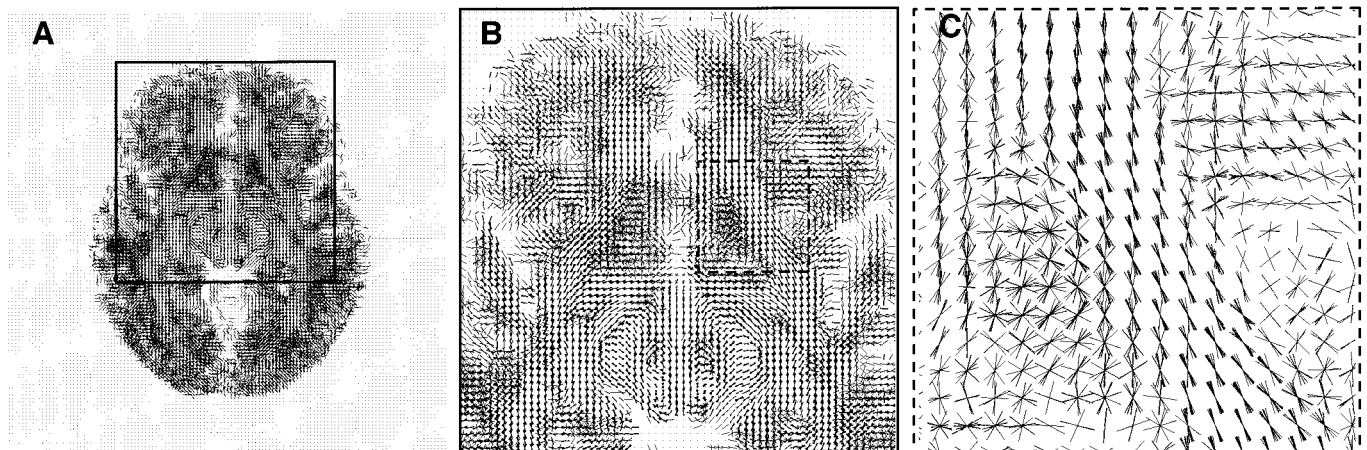

FIG. 10. Bow-tie plots of the principal eigenvectors in the subcortical white matter. The zoomed region selected in B and shown enlarged in C reveals a band of high coherence of the principal eigenvectors, in the location of the uncinate and inferior occipitofrontal fasciculi.
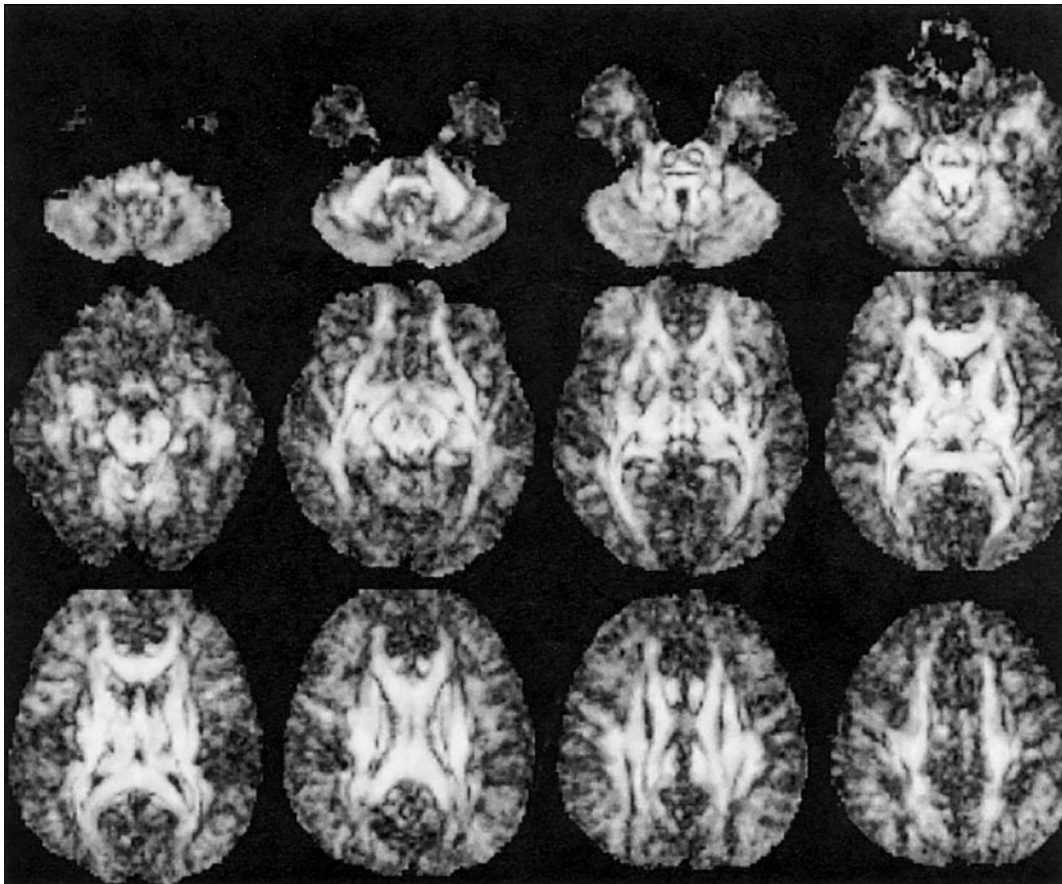
FIG. 11. Dyadic coherence map. Every third slice of the 60-slice image is shown. In each voxel, the intensity is directly proportional to the dyadic coherence, κ, formed according to Eq. (6).

Since we have been able to preserve orientational information during the group averaging procedure reported here, there now exists the potential for examining statistical differences in eigenvectors. While no framework currently exists for comparing such data in the DT-MRI literature, analytical techniques developed in other fields (Fisher *et al.,* 1953; Bingham *et al.,* 1974; Mardia, 1972) may offer approaches that are applicable for group analyses of eigenvector data.

As for tensorial data, we do not know of any statistical techniques for the analysis of these. However, it is felt that group analyses that consider the tensor as a whole (rather than in some collapsed form), either involving statistical comparison of tensors on a local basis or topological comparison of the tensor fields on a global basis (Hesselink *et al.,* 1997), may provide a more complete means for comparing two groups of subjects. Comparisons of tensor fields on a global basis may well help to crystallize group statistical differences into one or two readily interpretable figures/maps.

One thing is clear: caution should be exercised when interpreting results obtained by applying existing sta-

tistical techniques, designed for Gaussian distributed scalar variables, to scalar measures derived from diffusion tensor data in an *ad hoc* way, until it has been demonstrated that the data support their use. While such investigations are under way with the data collected for this study, they are beyond the scope of this paper.

Figure 6b shows that the median normalized standard deviation of tensors was 22%. This value can be used to estimate the number of subjects that would be required in order to detect systematic variations in anatomy by comparing diffusion tensor data. First, consider testing for variation at the level of a single voxel. Suppose we have two groups and that a real systematic difference exists between the anatomies of the two groups at the voxel in question. Assuming normally distributed statistics, we can determine the number of subjects that would be needed to detect this difference reliably over and above the 22% natural variation. If the anatomic difference gives rise to a 10% difference between the "within-group mean tensors," we can calculate that 27 subjects in each group would be needed in order to achieve 95% certainty of detec-
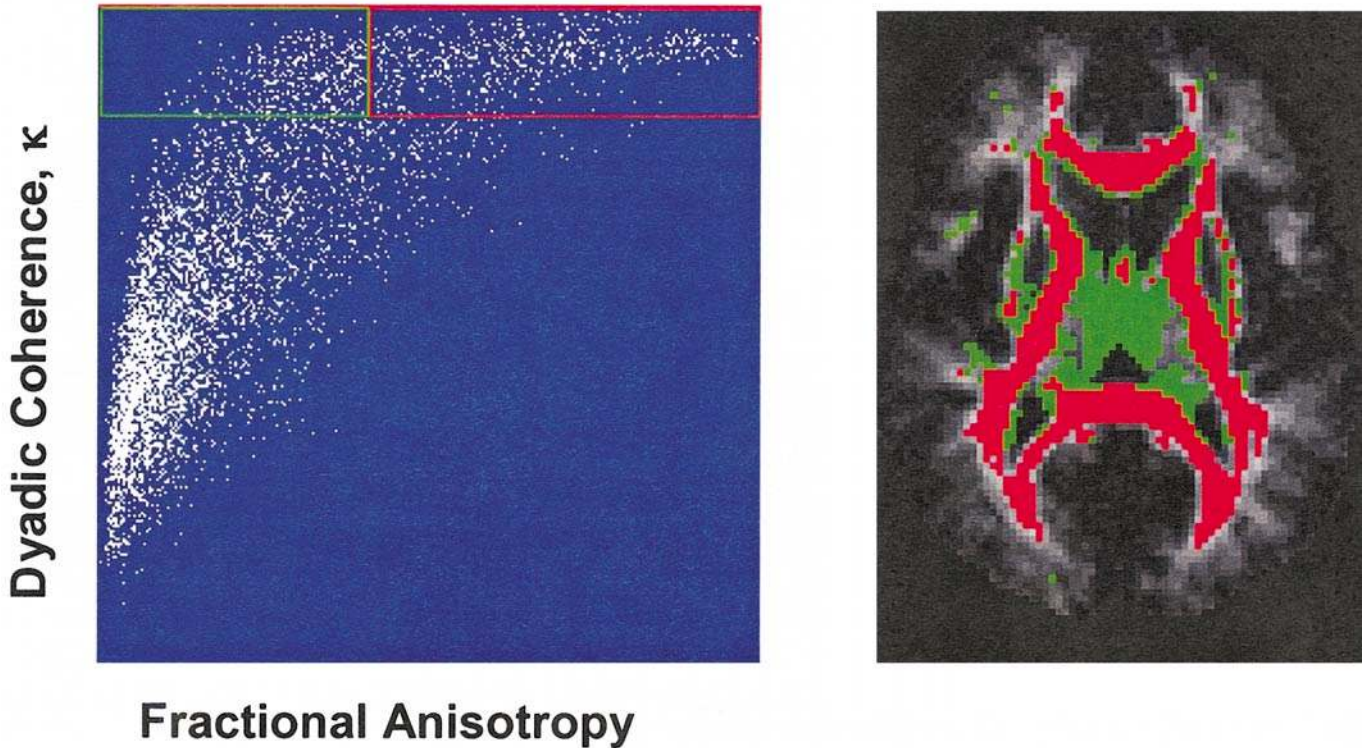
FIG. 12. Scattergram of dyadic coherence and fractional anisotropy data. The boundaries of two regions of interest were arbitrarily selected on the scattergram to select a region of "high" dyadic coherence and "high" fractional anisotropy (ROI and voxels shown in red) and a region of "high" dyadic coherence and "low" fractional anisotropy (ROI and voxels shown in green). The voxels are highlighted on an image of the fractional anisotropy.

tion. If the anatomic difference was as low as 5%, then 105 subjects would be needed in each group and if it was as high as 20%, only 7 subjects would be required in each group to achieve 95% confidence of detection of a difference.

Two points of caution regarding these calculations should be raised. First, the statistics will change when testing at multiple voxels in an effort to localize systematic anatomical differences. Second, the casual mixing of horizontal (registration) and vertical (within
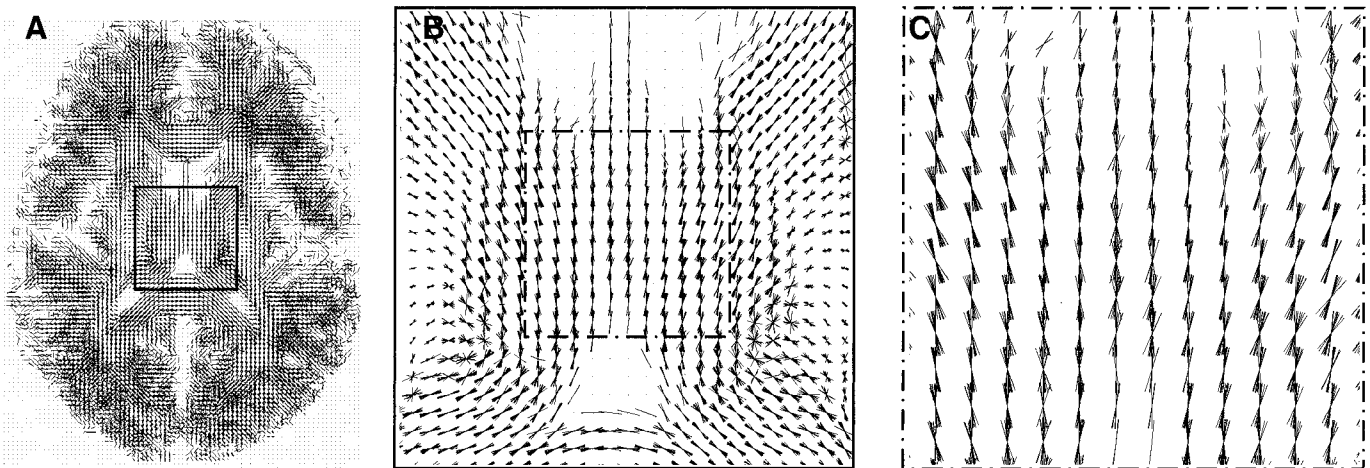

FIG. 13. Bow-tie plots of the principal eigenvectors in the thalamus. The square in (A) shows the approximate location of the zoomed region shown in (B), selected to examine orientational coherence in the thalamus. The region enclosed by the square in (B) has been enlarged in (C).

voxel, across subjects) analyses of anatomical images may be statistically suspect (Ashburner and Friston, 2001; Bookstein, 2001).

Orientational Coherence

One of the key points of this work was the development of techniques for examining intersubject intravoxel orientational coherence of eigenvectors in a group of spatially normalized DT-MRI data sets. These techniques may be of assistance when trying to draw inferences about "connectivity" in the brain by studying group-averaged (scalar) anisotropy data. In regions where the underlying intersubject coherence of eigenvectors is low, the significance of changes in the group-averaged anisotropy is difficult to interpret (Virta *et al.,* 1999). Some studies have suggested that changes in anisotropy indicate changes in functional connectivity (e.g., Buchsbaum *et al.,* 1998). However, even when the anisotropy of the tensor within a voxel across subjects within a subject group is similar, the intersubject coherence of fiber orientation within the voxel can be low, reflecting occupation of the voxel by different tracts. Therefore, a change in anisotropy in the voxel would be reflecting changes in anisotropy in different tracts. Hence, it is not clear that disruption to the fibers passing through the voxel will affect functional connectivity in the subjects in the same way.

It is our opinion that the orientational coherence of the underlying tensors must be considered simultaneous with measures of anisotropy when attempting to infer disruptions to connectivity from DT-MRI data. We also suggest that measures of intersubject orientational coherence could also be used in the design of studies, so that hypotheses about changes in diffusion tensor data can be tested more rigorously by aiding appropriate placement of ROIs (perhaps within a particular fasciculus), rather than by blindly placing a region of interest in, for example, "frontal" white matter.

The finding that the intersubject orientational coherence of the principal eigenvector was high, even though the anisotropy was low, in certain regions of the thalamus is intriguing. This could be partly attributable to the fact that the thalamus is a central structure and, as such, is likely to be more correctly coregistered with the affine approach employed here, than more peripheral structures. However, this explanation is unlikely to fully account for the high degree of orientational coherence seen in the thalamus. While DT-MRI studies involving group analyses have previously concentrated on white matter (Buchsbaum *et al.,* 1998; Hedehus *et al.,* 1999; Klingberg *et al.,* 1999; Lim *et al.,* 1999; Pfefferbaum *et al.,* 1999; Foong *et al.,* 2000; Steel *et al.,* 2001; Agartz *et al.,* 2001), the results obtained here suggest that intergroup comparisons of scalar, vector, and tensor measures in the thalamus may be possible.

Wiegell *et al.* have shown how individual thalamic nuclei can be identified visually (Wiegell *et al.,* 1999, 2000a) or automatically (Wiegell *et al.,* 2000b) using DT-MRI data. Even with the image of $\langle \mathbf{D} \rangle_2$, different regions of the thalamus have a specific pattern of anisotropy and dyadic coherence (Fig. 12), suggesting that the dyadic coherence measure may be useful as an additional measure for identifying different nuclei in a group of subjects.

By coupling Wiegell's approach with the DT-MRI spatial normalization and averaging presented here, it may even be possible to infer intergroup differences in individual thalamic nuclei.

Coregistration

For the data in this study, affine registration appears to be reasonably effective in preserving information in central structures. However, information in peripheral structures and end termini of central structures was poorly preserved. Furthermore, it should be noted that we selected a group of normal subjects with an age range of 33.3 ± 4.7 years, which was drawn from our colleagues. In older or diseased subjects, differing degrees of brain atrophy will complicate the registration used for spatial normalization. To ameliorate these problems, more sophisticated higher order coregistration such as polynomial or elastic registration techniques (Gee and Bajesy, 1998) coupled with the tensor reorientation strategies of Alexander *et al.* (1999, 2001a,b) may be beneficial, and this is an active area of our ongoing research. However, Alexander and Gee (2000) have observed that when higher order transformations are used for registration, the effects of noise can cause unpredictable reorientation of the tensors. The effects of noise can lead to high spatial frequency information being introduced even in homogeneous regions. The displacement field for registration can therefore contain spurious ridges and whorls. In such cases, using the information contained within the jacobian of the displacement field can lead to variable reorientations of the diffusion tensor, even in fairly homogeneous regions. Affine transformations are less susceptible to such noise effects, since the optimization of the transformation field is driven by macroscopic features of the image and the jacobian of the displacement field is constant. In view of these considerations, we have currently limited ourselves to affine registration, under which reorientation of tensors is known to be reliable (Alexander *et al.,* 2001).

We are also currently investigating the use of the dyadic coherence measure, κ, to drive the coregistration procedure (i.e., such that the global dyadic coherence is maximized). This is with the specific aim of improving tractography results obtained from an averaged DT-MRI data set, using a tractography algorithm that uses the principal eigenvector (as opposed to the

whole tensor) for determining the route of path propagation.

Finally, in this work spatial normalization was performed on the anisotropy images alone. It is possible, in principle, to perform the registration using all components of the tensor, rather than an index which represents one property of the tensor in a collapsed form (such as the anisotropy measure used here). Future studies will investigate this possibility and examine whether any bias is introduced by normalization based on the anisotropy alone.

Tractography

Our results indicate that it is possible to perform tractography in an averaged tensor data set and obtain plausible results in some major white matter fasciculi. In particular, results obtained in portions of centrally located fasciculi, where the intervoxel coherence of fiber orientation (both at the intra- and at the intersubject level) is high, appear to agree well between the mean and the individual data sets. These sections of the fasciculi are referred to as the "stems" by earlier workers (Makris *et al.,* 1997). In regions where the tracts diverge from the stem, or in small structures (such as the commissural fibers of the anterior commissure or end termini of fasciculi), the increased intersubject variability in white matter tract location and geometry means coregistration of these structures performs less well and so the tractography results obtained in the mean data set are likely to be less representative of the individual data sets, at least with this affine approach. Since these structures represent the end termini of connections between different regions of the brain, they are important for studying brain connectivity, and it is therefore essential that this issue is resolved if group-averaged maps are to be used to assess intergroup differences in connectivity.

Figure 14 demonstrates that tractography results obtained from the mean of 10 affine-coregistered subjects agree reasonably well, at least qualitatively, with results obtained in an individual data set, in major centrally located structures. In smaller structures, or where tracts extend to peripheral regions of the brain, the correlation between results obtained in the mean and individual data sets appears less strong.

There have been many reports of successful tracking of isolated tracts in the literature. The success of tracking central isolated structures such as the callosal fibers in the average brain, presented in Figs. 14a and 14b, may therefore not be too surprising. Such a result is encouraging for the study of the corpus callosum in schizophrenia, as several studies (e.g., Foong *et al.,* 2000; Agartz *et al.,* 2001) have reported differences in scalar DT-MRI measures between schizophrenics and controls. It may now be possible to probe these differences further by comparing eigenvector, tensor, and tractography data.

For application of DT-MRI to cognitive and psychiatric disorders in general, however, it would be interesting to focus not only on such structures as the corpus callosum, but also on the association pathways that typically run in the deep white matter of the hemispheres and which do not have well-defined and isolated trajectories. However, one may fear that the anatomical variability in the deep white matter may make meaningful tracking of the association pathways in a population-averaged brain impossible. Contrary to these concerns, we have been able to demonstrate that tractography results obtained from the group-averaged data set correlate well with results from an individual data set in the association pathways, such as the uncinate and inferior occipitofrontal fasciculi (Fig. 14c).

Figure 14d provides an important illustration of the differences between results obtained in the individual and mean brains. The intersubject/intravoxel orientational coherence in the region where the seed points were defined is low, which could be due to poorer performance of the spatial normalization in this area, or due to greater intersubject anatomical variability, or due to the principal eigenvector being poorly defined in the voxel for each subject (as a result of lower anisotropy)—or a combination of all three. This intersubject variability in results cannot be accurately reflected by the results obtained in the mean brain. Indeed, much smoother fiber trajectories are observed in the mean brain compared to the individual results. This example serves to show that extreme caution must be exerted when interpreting results obtained in the average brain in regions where the orientational coherence of principal eigenvectors is low.

If registration/normalization of the whole data set can be shown to be effective over the entire brain (perhaps using high-order elastic matching), the group-averaged data set could be used to generate a generic connectogram—a template which characterizes the routes and connections of fasciculi within a certain population.

We are currently investigating ways of quantifying just how representative a group-averaged tractography result is of the underlying subject data. One avenue that we are pursuing is to integrate the measures of intersubject agreement (either through the dyadic coherence measure, Eq. (6), or through the tensor dispersion measures, Eqs. (8) and (10)) along the tract. This would provide an assessment of the "confidence" we can assign to the tract of its ability to represent properties of the individual diffusion tensor fields.

In this work, we have not addressed the issue of choice of tractography algorithm since our aim was simply to investigate the feasibility of obtaining a tractography result on a group-averaged DT-MRI data set. The approach adopted here was to employ only the
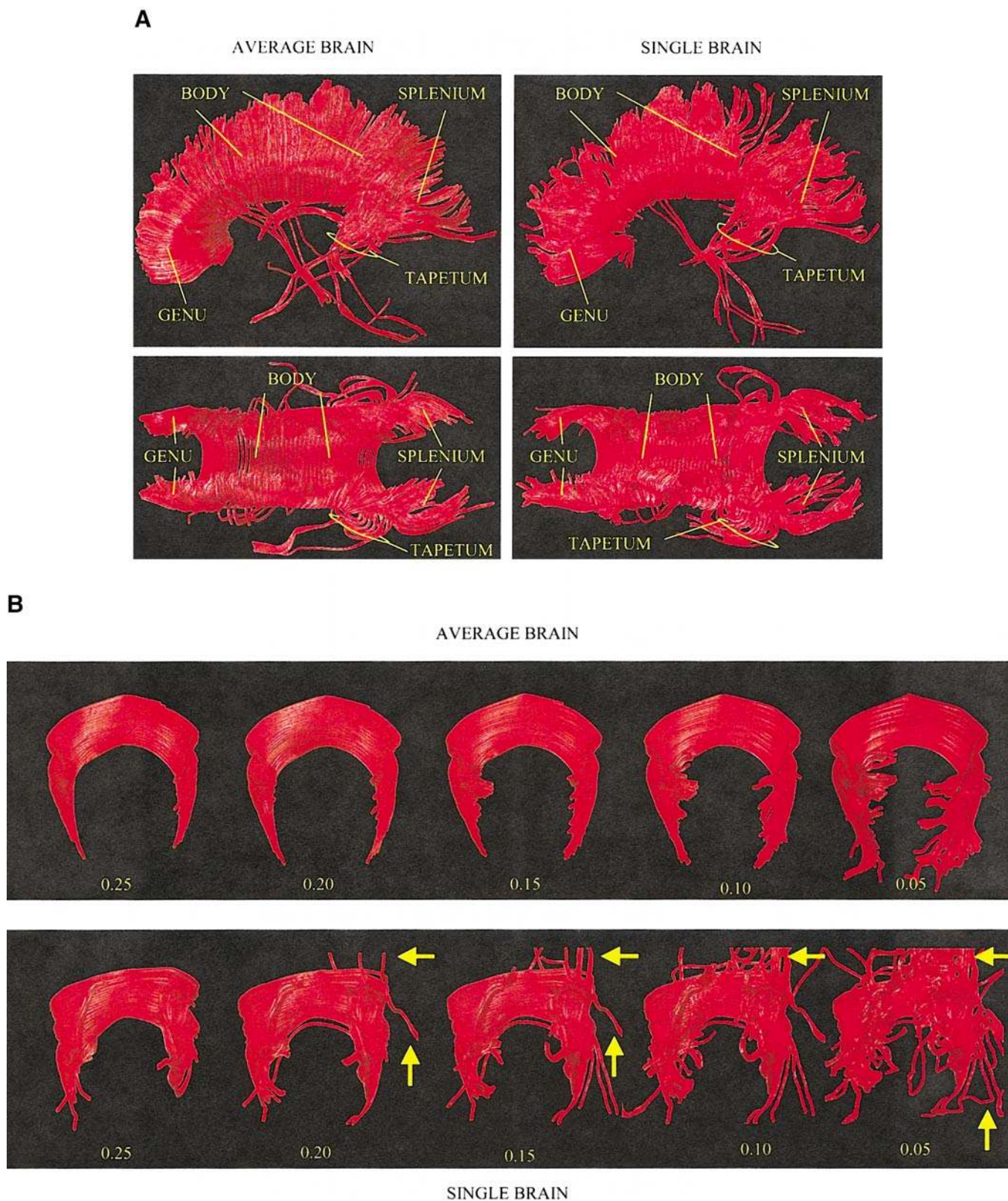
FIG. 14. Tractography results obtained from the mean-averaged diffusion tensor, $\langle D \rangle_2$, and individual data sets in: (A) The genu, body, splenium, and tapetum of the corpus callosum. (B) The anterior forcep of the corpus callosum, using different fractional anisotropy thresholds. The yellow arrows point to spurious reconstructed fiber trajectories that do not belong to the anterior forcep of the corpus callosum. (C) The uncinate fasciculus (green) and the inferior fronto-occipital fasciculus (red) obtained in the mean and individual data sets. The yellow lines on the sagittal views show the locations of the axial sections on which ROIs were drawn to "dissect" the fasciculi from each other using a two-ROI approach. For both the mean and the individual brain, the same region of interest was used for initiation of tracking (defined on slice 1). The ROIs used to detect the uncinate and inferior fronto-occipital fasciculi are shown in green and red, respectively. (D) The frontal white matter region highlighted in Fig. 9A.
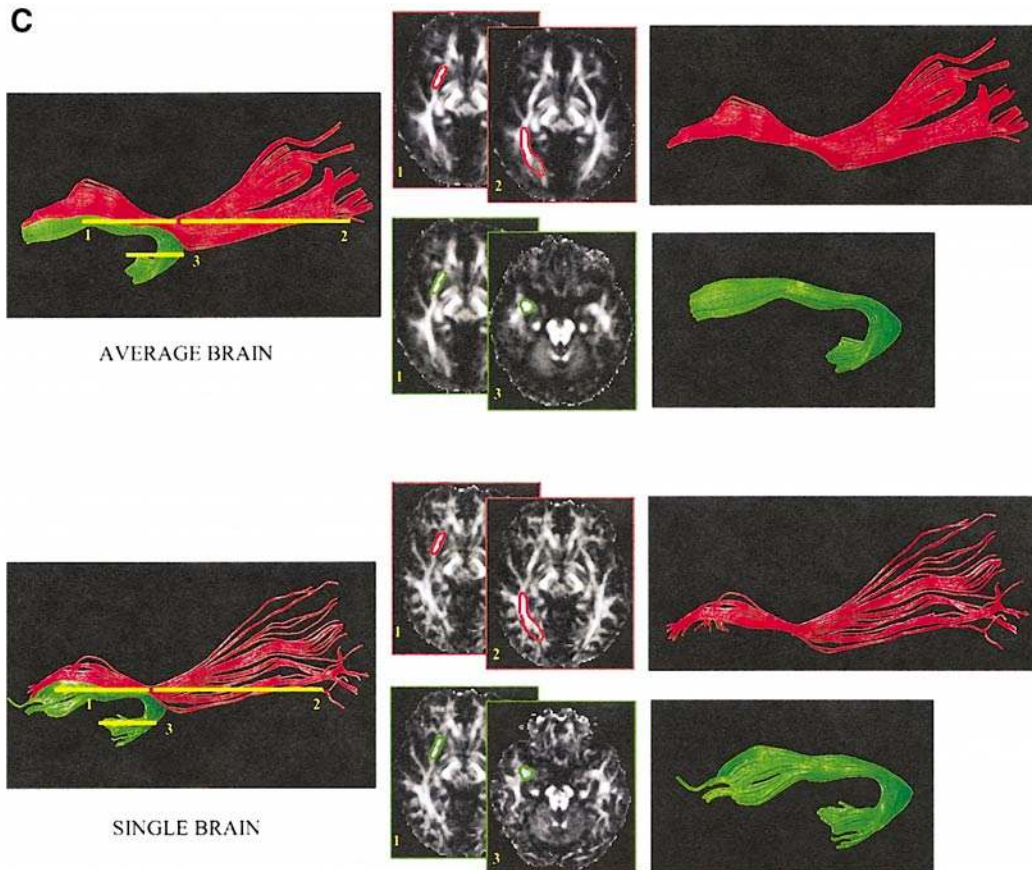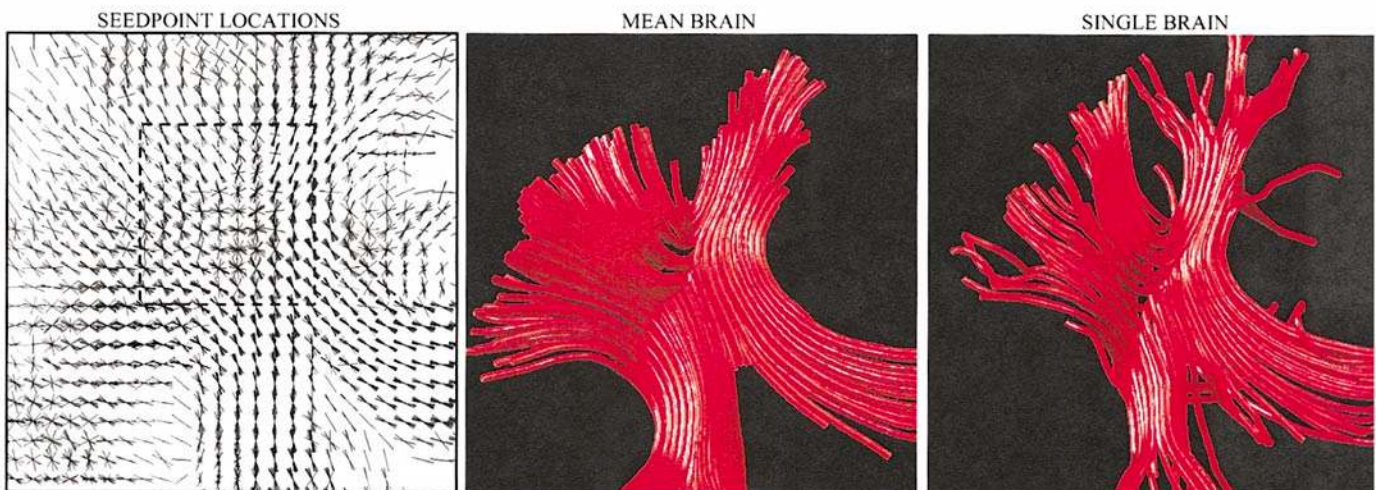
C

AVERAGE BRAIN

SINGLE BRAIN

D

SEEDPOINT LOCATIONS

MEAN BRAIN

SINGLE BRAIN

FIG. 14—*Continued*

directional information contained within the principal eigenvector, which is taken to be parallel to the dominant orientation of fibers within the voxel. When the orientational coherence of the fibers within a voxel is high, then we expect the principal eigenvector to correctly indicate the fiber orientation within the voxel. However, when the fiber orientational coherence is

low, for example if fibers splay out or if fibers cross within a voxel, then the principal eigenvector of the voxel-averaged diffusion tensor can no longer accurately reflect the underlying fiber orientations. While the diffusion tensor is adequate to characterize diffusion when the diffusion displacement profile is Gaussian, these complex structures give rise to significant

deviations from a Gaussian diffusion displacement profile. Recent work (Tuch *et al.,* 1999; Wedeen *et al.,* 2000; Alexander *et al.,* 2001; Frank, 2001; Alexander *et al.,* 2001a,b) has investigated higher order, non-Gaussian representations of diffusion in complex tissue, as a means of more completely characterizing diffusion. Incorporating these techniques into a tractography algorithm would undoubtedly improve its robustness in regions of low intravoxel directional coherence and may help to tease out connectivity information in subcortical regions both in individual subject data and in the group-averaged data. An interesting question, then, is how well the methods described here (where a single tensor model has been used) could be extended to cases in which more complex non-Gaussian descriptions are used. In general, a methodology similar to that described in this paper could be applied to images that contain non-Gaussian descriptions of the displacement due to diffusion, in order to investigate their intersubject variability in particular regions. Some investigation would be required to extend the methods described by Alexander *et al.* (2001, 2002) to cope with these representations.

The Benefits of Warping DT-MRI Data to a Common Reference Frame

As the use of diffusion tensor imaging becomes increasingly widespread, it will be used as a tool to aid in a range of neuroscientific and clinical investigations. It is likely that the information obtained from DT-MRI will not be used in isolation, but will be used in conjunction with image data obtained from other MRI contrasts, for example T_1-weighted high-resolution structural data or functional MRI (fMRI) data. With these latter image contrasts, it is common practice to coregister the data to a common reference template such as that of Tailarach and Tournoux (1998). Fusion of DT-MRI data with these and other imaging modalities such as PET (e.g., Buchsbaum *et al.,* 1998) requires that DT-MRI data are coregistered to the same template. In this work, we have simply chosen a template which is commonly used throughout the fMRI community to illustrate how DT-MRI data can be mapped into a chosen reference template.

We note that if one is interested only in looking at rotationally invariant indices obtained from the diffusion tensor, such as the trace or measures of anisotropy (e.g., Basser and Pierpaoli, 1996), then it is not necessary to perform reorientation of the tensors. Rather, the tensors would be calculated in each individual and the rotationally invariant measures computed *prior* to applying the spatial transformation. However, the approach that is presented here allows one to look beyond scalar invariants and to compare eigenvectors between different subjects in a meaningful manner. Furthermore, it becomes possible to perform statistical comparisons of individual elements of the diffusion tensor between different subjects. Such comparisons would be meaningless unless the DT-MRI data are correctly transformed and reoriented in the manner described here. We speculate that examining the individual tensor elements may reveal more information than examining scalar invariants alone.

We note that an alternative approach to averaging the tensor data sets prior to tracking fasciculi would be to track fasciculi on the 10 individual data sets and then use the registration results simply to warp the path of these tracks onto the chosen template. The result of this latter approach would be something approximating a "probabilisitic" fiber map. However, the uncertainty in the reconstructed path due to the inherent noise can lead to deviations from the true path of the underlying fasciculus (which is true for all tractography approaches). Therefore, such a probabilistic map of fiber location would contain variability due to two sources: (a) variability which is due solely to MR noise and uncertainties in fiber orientation and (b) true anatomical variability. When viewing such an image, it would not be possible to determine what part of the variability is attributable to which effect.

On the other hand, the approach that we describe here does not make any provision for allowing anatomical or noise-induced variability in the trajectories of individual subjects to be determined. However, by averaging the individual tensors from the subjects *prior* to the tracking, the noise-induced variability is somewhat reduced, which is advantageous for picking out the tracts. This results in sharpness and improved definition of a number of the nerve pathways. In contrast to a fuzzy probabilistic map, we end up with a smooth and continuous trajectory which represents the "central" location of the tracts within the population.

CONCLUSION

We have shown how DT-MRI data sets can be spatially normalized to a standard anatomical reference space and have developed qualitative and quantitative techniques for assessing the results of spatial normalization.

Encouraging results were obtained even with a simple affine registration. Anisotropy and orientational information were remarkably well preserved in central regions of the brain when 10 individual DT-MRI data sets were combined, while in peripheral regions the wider range of intersubject anatomical variability and the choice of registration algorithm meant that such information was less well preserved. It is therefore envisaged that more sophisticated "elastic" registration algorithms could serve to improve results.

By spatially normalizing to, and averaging in, a standard anatomical template space, cross-referencing to images with other contrast, such as fMRI data, now

becomes feasible. However, we caution against the notion of currently being able to "explain" differences in functional connectivity measured by fMRI using information obtained from DT-MRI.

We have demonstrated that plausible tractography results may be obtained from major white matter fasciculi in group-averaged DT-MRI data sets. However, we have also shown, through the use of the bow-tie plots, that a tractography result obtained from subcortical regions in the average brain would not be very representative of the results obtained from individual subjects. Again, it is envisaged that this situation could be improved through the use of more sophisticated image registration algorithms.

Finally, while we have shown that spatial normalization of DT-MRI data sets is possible, and we have demonstrated for the first time how to determine measures of central tendency and scatter of a distribution of tensors. We have also highlighted the absence of, and need for, appropriate statistical techniques for making robust inferences about differences in group-averaged DT-MRI data sets between different subject groups. When such techniques have been developed, their combination with the spatial normalization and averaging procedures outlined here should increase the applicability of DT-MRI to, and enable more robust and meaningful interpretation of data from, a wider range of neurological and psychiatric investigations.

ACKNOWLEDGMENTS

REFERENCES

Agartz, I., Andersson, J. L. R., and Skare, S. 2001. Abnormal brain white matter in schizophrenia: A diffusion tensor imaging study. *NeuroReport* **12:** 2251–2254.

Aldroubi, A., and Basser, P. J. 1999. Reconstruction of vector and tensor fields from sampled discrete data. *Contemp. Math.* **247:** 1–15.

Alexander, A. L., Hasan, K. M., Lazar, M., Tsuruda, J. S., and Parker, D. L. 2001. Analysis of partial volume effects in diffusion-tensor MRI. *Magn. Reson. Med.* **45:** 770–780.

Alexander, D. C., Gee, J. C., and Bajesy, R. 1999. Strategies for data reorientation during non-rigid transformations of diffusion tensor

images. In *Proc. 2nd International Conference on Medical Image Computing and Computer-Assisted Intervention.*

Alexander, D. C., and Gee, J. C. 2000. Elastic matching of diffusion tensor images. *Comput. Vis. Image Und.* **77:** 233–250.

Alexander, D. C., Pierpaoli, C., Basser, P. J., and Gee, J. C. 2001a. Spatial transformations of diffusion tensor magnetic resonance images. *IEEE Trans. Med. Imaging* **20:** 1131–1139.

Alexander, D. C., Barker, G. J., and Arridge, S. R. 2002. Detection and modeling of non-Gaussian apparent diffusion coefficient profiles in human brain data. *Magn. Reson. Med.* **48:** 331–340.

Ashburner, J., and Friston, K. J. 2001. Why voxel-based morphometry should be used. *NeuroImage* **14:** 1238–1243.

Basser, P. J. 1998. Fiber-tractography via diffusion tensor MRI (DT-MRI) In *Book of Abstracts: Sixth Annual Meeting of the International Society for Magnetic Resonance in Medicine,* Vol. 2, p. 1226. Int. Soc. Magn. Reson. Med., Berkeley, CA.

Basser, P. J., Matiello, J., and Le Bihan, D. 1994. Estimation of the effective self-diffusion tensor from the NMR spin echo. *J. Magn. Reson. B* **103:** 247–254.

Basser, P. J., and Pierpaoli, C. 1995. Elucidating tissue structure by diffusion tensor MRI. In *Book of Abstracts: Third Annual Meeting of the International Society for Magnetic Resonance in Medicine,* Vol. 2, p. 900. Int. Soc. Magn. Reson. Med., Berkeley, CA.

Basser, P. J., and Pierpaoli, C. 1996. Microstructural and physiological features of tissue elucidated by quantitative-diffusion-tensor MRI. *J. Magn. Reson. B* **111:** 209–219.

Basser, P. J., and Pajevic, S. 2000. Statistical artefacts in diffusion tensor MRI (DT-MRI) caused by background noise. *Magn. Reson. Med.* **44:** 41–50.

Basser, P. J., Pajevic, S., Pierpaoli, C., Duda, J., and Aldroubi, A. 2000. In vivo tractography using DT-MRI data. *Magn. Reson. Med.* **44:** 625–632.

Bingham, C. 1974. An antipodally symmetric distribution on the sphere. *Ann. Stat.* **2:** 1201–1225.

Bookstein, F. 2001. Voxel-based morphometry should not be used with imperfectly registered images. *NeuroImage* **14:** 1454–1462.

Buchsbaum, M. S., Tang, C. Y., Peled, S., Gudbjartsson, H., Lu, D., Hazlett, E. A., Downhill, J., Haznedar, M., Fallon, J. H., and Atlas, S. W. 1998. MRI white matter diffusion anisotropy and PET metabolic rate in schizophrenia. *NeuroReport* **9:** 425–430.

Collingnon, A., Maes, F., Delaere, D., Vandermeulen, D., Suetens, P., and Marcha, G. 1995. Automated multimodality medical image registration using information theory. In *Proc. XIVth International Conference on Information Processing in Medical Imaging. Computational Imaging and Vision* Vol. 3, pp. 263–274.

Conturo, T. E., Lori, N. F., Cull, T. S., Akbudak, E., Snyder, A. Z., Shimony, J. S., McKinstry, R. C., Burton, M., and Raichle, M. E. 1999. Tracking neuronal fiber pathways in the living human brain. *Proc. Natl. Acad. Sci. USA* **96:** 10422–10427.

Crank, J. 1956. *The Mathematics of Diffusion.* Oxford Univ. Press, Oxford.

Crosby, E. C., Humphrey, T., and Lauer, E. W. 1962. *Correlative Anatomy of the Nervous System.* Macmillan Co., New York.

Dejerine, J. 1895. *Anatomie des Centres Nerveux,* Vol. 1. Rueff, Paris.

Dejerine, J. 1901. *Anatomie des Centres Nerveux,* Vol 2. Rueff, Paris.

Ellis, C. M., Simmons, A., Jones, D. K., Bland, J., Dawson, J. M., Horsfield, M. A., Williams, S. C. R., and Leigh, P. N. 1999. Diffusion tensor MRI assesses corticospinal tract damage in ALS. *Neurology* **53:** 1051–1058.

Eriksson, S. H., Symms, M. R., Barker, G. J., Wieshmann, U. C., Woermann, F. G., and Duncan, J. S. 1999. Investigation of white matter tracts in malformations of cortical development using MR diffusion tensor imaging and statistical parametric mapping. *NeuroImage* **9:** S562.

Eriksson, S. H., Rugg-Gunn, F. J., Symms, M. R., Barker, G. J., and Duncan, J. S. 2001. Diffusion tensor imaging in patients with epilepsy and malformations of cortical development. *Brain* **124:** 617–626.

Fisher, R. A. 1953. Dispersion on a sphere. *Proc. R. Soc. London A* **217:** 295–305.

Foong, J., Maier, M., Clark, C. A., Barker, G. J., Miller, D. H., and Ron, M. A. 2000. Neuropathological abnormalities of the corpus callosum in schizophrenia: A diffusion tensor imaging study. *J. Neurol. Neurosurg. Psychiatry* **68:** 242–244.

Frank, L. R. 2001. Anisotropy in high angular resolution diffusion-weighted MRI. *Magn. Reson.Med.* **45:** 935–939.

Frechet, M. 1948. Les elements aléatoires de nature quelconque dans un espace distancié. *Ann. Inst. Henri Poincaré* **X:** 215–308.

Friston, K. J., Holmes, A. P., Worsley, K. J., Poline, J. B., Frith, J. D., and Frackowiak, R. S. 1995a. Statistical parametric maps in functional imaging: A general linear approach. *Hum. Brain Mapp.* **2:** 189–210.

Friston, K. J., Ashburner, J., Frith, J. D., Poline, J. B., Heather, J. D., and Frackowiak, R. S. 1995b. Spatial registration and normalisation of images. *Hum. Brain Mapp.* **3:** 165–189.

Gee, J. C., and Bajcsy, R. K. 1998. Elastic matching: Continuum mechanical and probabilistic analysis. In *Brain Warping* (A. W. Toga, Ed.). Academic Press, San Diego.

Glauche, V., Sach, M., Koch, M., Heimbach, B., Winkler, G., Nolte, U., Finterbusch, J., Frahm, J., Weiller, C., and Büchel, C. 2001. Morphometry on diffusion tensor data. *NeuroImage* **13:** S128.

Griffin, L. D. 1997. Scale-imprecision space. *Image Vision Comput.* **15:** 369–398.

Hedehus, M., Sullivan, E. V., de Crespigny, A., Moseley, M. E., Lim, K. O., and Pfefferbaum, A. 1999. Low white matter anisotropy in chronic alchoholism revealed with diffusion tensor imaging. In *Book of Abstracts: Seventh Annual Meeting of the International Society for Magnetic Resonance in Medicine,* Vol. 2, p. 932. Int. Soc. Magn. Reson. Med., Berkeley, CA.

Hesselink, L., Levy, Y., and Lavin, Y. 1997. The topology of symmetric, second-order 3D tensor fields. *IEEE Trans. Visualisat. Comput. Graph.* **3:** 1–11.

Holmes, A. P., Blair, R. C., Watson, J. D. G., and Ford, I. 1996. Nonparametric analysis of statistic images from functional mapping experiments. *J. Cereb. Blood Flow Metab.* **16:** 7–22.

Jones, D. K., Simmons, A., Williams, S. C. R., and Horsfield, M. A. 1998. Non-invasive assessment of structural connectivity in white matter by diffusion tensor MRI. In *Book of Abstracts: Sixth Annual Meeting of the International Society for Magnetic Resonance in Medicine,* Vol. 1, p. 531. Int. Soc. Magn. Reson. Med., Berkeley, CA.

Jones, D. K., Simmons, A., Williams, S. C. R., and Horsfield, M. A. 1999a. Non-invasive assessment of axonal fiber connectivity in the human brain via diffusion tensor MRI. *Magn. Reson. Med.* **42:** 37–41.

Jones, D. K., Horsfield, M. A., and Simmons, A. 1999b. An optimal strategy for precise determination of the diffusion tensor. In *Book of Abstracts: Sixth Annual Meeting of the International Society for Magnetic Resonance in Medicine,* Vol. 3. p. 1793. Int. Soc. Magn. Reson. Med., Berkeley, CA.

Jones, D. K., Horsfield, M. A., and Simmons, A. 1999c. Optimal strategies for measuring diffusion in anisotropic systems by magnetic resonance imaging. *Magn. Reson. Med.* **42:** 515–525.

Jones, D. K., Williams, S. C. R., Gasston, D., Horsfield, M. A., Simmons, A., and Howard, R. 2002. Isotropic resolution diffusion tensor imaging with whole brain acquisition in a clinically acceptable time. *Hum. Brain Mapp.* **15:** 216–230.

Klingberg, T., Hedehus, M., Temple, E., Salz, T., Gabrieli, J. D. E., Moseley, M. E., and Poldrack, R. A. 2000. Microstructure of temporo-parietal white matter as a basis for reading ability: Evidence from diffusion tensor magnetic resonance imaging. *Neuron* **25:** 493–500.

Koch, M., Glauche, V., Finsterbusch, J., Nolte, U., Frahm, J., and Büchel, C. 2001. Estimation of anatomical connectivity from diffusion tensor data. *NeuroImage* **13:** S176.

Lim, K. O., Hedehus, M., Moseley, M. E., de Crespigny, A., Sullivan, E. V., and Pfefferbaum, A. 1999. Compromised white matter tract integrity in schizophrenia inferred from diffusion tensor imaging. *Arch. Gen. Psychiatry* **56:** 367–374.

Makris, N., Worth, A. J., Sorensen, A. G., Papadimitriou, G. M., Wu, O., Reese, T. G., Wedeen, V. J., Davis, T. L., Stakes, J. W., Caviness, V. S., Kaplan, E., Rosen, B. R., Pandya, D. N., and Kennedy, D. N. 1997. Morphometry of in vivo human white matter association pathways with diffusion-weighted magnetic resonance imaging. *Ann. Neurol.* **42:** 951–962.

Mardia, K. V. 1972. *Statistics of Directional Data.* Academic Press, London.

Mori, S., Crain, B. J., and van Zijl, P. C. 1998. 3D brain fiber reconstruction from diffusion MRI. In *Proceedings of the International Conference on Functional Mapping of the Human Brain,* Montreal, 1998.

Mori, S., Crain, B. J., Chacko, V. P., and van Zijl, P. C. 1999. Three dimensional tracking of axonal projections in the brain by magnetic resonance imaging. *Ann. Neurol.* **45:** 265–269.

Morse, P. M., and Feschbach, H. 1953. *Methods of Theoretical Physics.* McGraw–Hill, New York.

Moseley, M. E., Cohen, Y., Kucharczyk, J., Mintorovitch, J., Agari, H. S., Wendland, H. F., Tsuruda, J., and Norman, D. 1990. Diffusion-weighted MR imaging of anisotropic water diffusion in cat central nervous system. *Radiology* **176:** 439–445.

Pajevic, S., and Pierpaoli, C. 1999a. Color schemes to represent the orientation of anisotropic tissues from diffusion tensor data: Application to white matter fiber tract mapping in the human brain. *Magn. Reson. Med.* **42:** 526–540.

Pajevic, S., and Basser, P. J. 1999b. Parametric description of noise in diffusion tensor MRI. In *Book of Abstracts: Seventh Annual Meeting of the International Society for Magnetic Resonance in Medicine,* Vol. 3, p. 1787. Int. Soc. Magn. Reson. Med., Berkeley, CA.

Pajevic, S., and Pierpaoli, C. 2000. Color schemes to represent the orientation of anisotropic tissues from diffusion tensor data: Application to white matter fiber tract mapping in the human brain. *Magn. Reson. Med.* **43:** 921–921.

Pajevic, S., Basser, P. J., and Aldroubi, A. 2001. A continuous tensor field approximation for DT-MRI data. In *Book of Abstracts: Seventh Annual Meeting of the International Society for Magnetic Resonance in Medicine,* Vol. 2, p. 1535. Int. Soc. Magn. Reson. Med., Berkeley, CA.

Parker, G. J. M., Wheeler-Kingshott, C. A., and Barker, G. J. 2001. Distributed anatomical connectivity derived from diffusion tensor imaging. In *Proc Information Processing in Medical Imaging IMPI'01, Lecture Notes in Computer Science,* pp. 106–120. Springer-Verlag, Berlin.

Pennec, X., and Ayache, N. 1998. Uniform distribution, distance and expectation problems for geometric features processing. *J. Math. Imaging Vision* **9:** 49–67.

Pfefferbaum, A., Sullivan, E. V., Hedehus, M., Moseley, M., and Lim, K. O. 1999. Brain gray and white matter transverse relaxation time in schizophrenia. *Psychiatry Res. Neuroimaging* **91:** 93–100.

Pierpaoli, C., and Basser, P. J. 1996. Towards a quantitative assessment of diffusion anisotropy. *Magn. Reson. Med.* **36:** 893–906.

Poupon, C., Clark, C. A., Frouin, V., Regis, J., Bloch, I., Le Bihan, D., and Mangin, J. 1999. Tracking white matter fasciculi with diffusion tensor imaging. In *Book of Abstracts: Seventh Annual Meeting*

of the International Society for Magnetic Resonance in Medicine, Vol. 1, p. 325. Int. Soc. Magn. Reson. Med., Berkeley, CA.

Poupon, C., Clark, C. A., Frouin, V., Regis, J., Bloch, I., Le Bihan, D., and Mangin, J. 2000. Regularization of diffusion-based direction maps for the tracking of brain white matter fasciculi. *NeuroImage* **12:** 184–195.

Press, W. H., Teukolsky, S. A., Vetterling, W. T., and Flannery, B. P. 1992. *Numerical Recipes in C: The Art of Scientific Computing.* Cambridge Univ. Press, New York.

Rugg-Gunn, F. J., Eriksson, S. H., Symms, M. R., Barker, G. J., and Duncan, J. S. 2001. Diffusion tensor imaging of cryptogenic and acquired partial epilepsies. *Brain* **124:** 627–636.

Steel, R. M., Bastin, M. E., McConnell, S., Marshall, I., Cunnigham-Owens, D. G., Lawrie, S. M., Johnstone, E. C., and Best, J. J. K. 2001. Diffusion tensor imaging (DTI) and proton magnetic resonance spectroscopy (^{1}H MRS) in schizophrenic subjects and normal controls. *Psychiatry Res. Neuroimaging.* **106:** 61–170.

Tailarach, J., and Tournoux, P. 1988. *Co-planar Stereotaxic Atlas of the Human Brain: 3 Dimensional Proportional System. An Approach to Cerebral Imaging.* Thieme, New York.

Tuch, D. S., Weisskoff, R. M., Belliveau, J. W., and Wedeen, V. J., 1999. High angular resolution diffusion imaging of the human brain. In *Book of Abstracts: Seventh Annual Meeting of the International Society for Magnetic Resonance in Medicine,* Vol. 1, p. 321. Int. Soc. Magn. Reson. Med., Berkeley, CA.

Tuch, D. S., Belliveau, J. W., and Wedeen, V. J. 2000. A path integral approach to white matter tractography. In *Book of Abstracts: Eighth Annual Meeting of the International Society for Magnetic Resonance in Medicine,* Vol. 2. p. 791. Int. Soc. Magn. Reson. Med., Berkeley, CA.

Tuch, D. S., Wiegell, M. R., Reese, T. G., Belliveau, J. W., and Wedeen, V. J. 2001. Measuring cortico-cortical connectivity matrices with diffusion spectrum imaging. In *Book of Abstracts: Ninth Annual Meeting of the International Society for Magnetic Resonance in Medicine,* Vol. 1, p. 502. Int. Soc. Magn. Reson. Med., Berkeley, CA.

Viola, P., and Wells, W. M., III. 1996. Multi-modal volume registration by maximization of mutual information. *Med. Image Anal.* **1:** 35–51.

Virta, A., Barnett, A., and Pierpaoli, C. 1999. Visualizing and characterizing white matter fiber structure and architecture in the human pyramidal tract using diffusion tensor MRI. *Magn. Reson. Imaging* **17:** 1121–1133.

Wedeen, V. J., Reese, T. G., Tuch, D. S., Weigell, M. R., Dou, J.-G., Weisskoff, R. M., and Chesler, D. 2000. Mapping fiber orientation spectra in cerebral white matter with Fourier transform diffusion MRI. In *Book of Abstracts: Eighth Annual Meeting of the International Society for Magnetic Resonance in Medicine,* Vol. 1, Int. Soc. Magn. Reson. Med., Berkeley, CA. p. 82.

Wiegell, M. R., Larsson, H. B. W., and Wedeen, V. J. 1999. Diffusion tensor MRI of the thalamus: Differentiation of nuclei by their projections. In *Book of Abstracts: Seventh Annual Meeting of the International Society for Magnetic Resonance in Medicine,* Vol. 2, p. 934. Int. Soc. Magn. Reson. Med., Berkeley, CA.

Wiegell, M. R., Tuch, D. S., Larsson, H. B. W., and Wedeen, V. J. 2000a. Angular differentiation of thalamic nuclei by quantitative DTI. In *Book of Abstracts: Eighth Annual Meeting of the International Society for Magnetic Resonance in Medicine,* Vol. 1, p. 481. Int. Soc. Magn. Reson. Med., Berkeley, CA.

Wiegell, M. R., Tuch, D. S., Larsson, H. B. W., and Wedeen, V. J. 2000b. Automatic identification of thalamic nuclei from DTI. In *Proceedings of the Sixth Annual Meeting of the Organization for Human Brain Mapping,* p. 453.

Woods, R. P., Grafton, S. T., Holmes, C. J., Cherry, S. R., and Mazziotta, J. C. 1998a. Automated image registration. I. General methods and intra-subject and intra-modality validation. *J. Comput. Assisted Tomogr.* **22:** 141–154.

Woods, R. P., Grafton, S. T., Holmes, C. J., Cherry, S. R., and Mazziotta, J. C. 1998b. Automated image registration. II. Inter-subject validation of linear and non-linear models. *J. Comput. Assisted Tomogr.* **22:** 155–165.

Zhang, S., Curry, C., Morris, D. S., and Laidlaw, D. H. 2000. Visualizing diffusion tensor MR images using streamtubes and streamsurfaces. In *Proceedings of the IEEE Visualization Conference,* Utah.